Monthly Notices of the ROYAL ASTRONOMICAL SOCIETY

MNRAS **525,** 561–576 (2023)
Advance Access publication 2023 July 27

https://doi.org/10.1093/mnras/stad2273

Constraints on the Galactic centre environment from *Gaia* hypervelocity stars III: insights on a possible companion to Sgr A*

F. A. Evans [1,2]★ A. Rasskazov,[3] A. Remmelzwaal,[4] T. Marchetti [5] A. Castro-Ginard,[4] E. M. Rossi[4] and J. Bovy [1,2]

[1]*David A. Dunlap Department of Astronomy and Astrophysics, University of Toronto, 50 St. George Street, Toronto, ON M5S 3H4, Canada*
[2]*Dunlap Institute for Astronomy and Astrophysics, University of Toronto, 50 St. George Street, Toronto, ON M5S 3H4, Canada*
[3]*DAMTP, University of Cambridge, CMS, Wilberforce Road, Cambridge CB3 0WA, UK*
[4]*Leiden Observatory, Leiden University, PO Box 9513, NL-2300 RA Leiden, the Netherlands*
[5]*European Southern Observatory, Karl-Schwarzschild-Strasse 2, D-85748 Garching bei München, Germany*

Accepted 2023 July 19. Received 2023 July 6; in original form 2023 April 24

ABSTRACT

We consider a scenario in which Sgr A* is in a massive black hole binary (MBHB) with an as-of-yet undetected supermassive or intermediate-mass black hole companion. Dynamical encounters between this MBHB and single stars in its immediate vicinity would eject hypervelocity stars (HVSs) with velocities beyond the Galactic escape velocity of the Galaxy. In this work, we use existing HVS observations to constrain for the first time the existence of a companion to Sgr A*. We simulate the ejection of HVSs via the 'MBHB slingshot' scenario and show that the population of HVSs detectable today depends strongly on the companion mass and the separation of the MBHB. We demonstrate that the lack of uncontroversial HVS candidates in *Gaia* Data Release 3 places a firm upper limit on the mass of a possible Sgr A* companion. Within one milliparsec of Sgr A*, our results exclude a companion more massive than 2000 $M_\odot$. If Sgr A* recently merged with a companion black hole, our findings indicate that unless this companion was less massive than 500 $M_\odot$, this merger must have occurred at least 10 Myr ago. These results complement and improve upon existing independent constraints on a companion to Sgr A* and show that large regions of its parameter space can now be ruled out.

Key words: stars: kinematics and dynamics – Galaxy: centre – Galaxy: nucleus – black hole mergers.

1 INTRODUCTION

In the centre of our Galaxy lurks *Sagittarius A** (Sgr A*), a supermassive black hole (SMBH) with a mass of $\sim 4 \times 10^6\,M_\odot$ (Ghez et al. 2008; Genzel, Eisenhauer & Gillessen 2010; Akiyama et al. 2022). Such SMBHs seem to be omnipresent in the nuclei of external galaxies as well (Magorrian et al. 1998; Kormendy & Ho 2013), at least among galaxies above a particular mass (see Merritt 2013). The hierarchical nature of structure formation in our Universe and the impact of dynamical friction (Chandrasekhar 1943) in dense stellar systems imply that major galaxy mergers result in bound SMBH–SMBH binaries (e.g. Begelman, Blandford & Rees 1980; Volonteri, Haardt & Madau 2003; Di Matteo, Springel & Hernquist 2005). These binaries have received considerable attention in recent years owing to the fact that inspiralling and colliding SMBH–SMBH binaries are loud gravitational wave sources (Peters 1964) in a frequency range accessible to the upcoming Laser Interferometer Space Antenna (LISA; Amaro-Seoane et al. 2017).

If Sgr A* were in a SMBH–SMBH binary in our own Galactic centre (GC), there would be clear observational signatures. In recent years, astrometric observations of Sgr A* (e.g. Reid & Brunthaler 2004, 2020) and kinematic analyses of the S-star cluster in the vicinity of the GC (e.g. Gualandris & Merritt 2009; Naoz et al. 2020; GRAVITY Collaboration et al. 2023) have excluded this notion. However, the possibility of Sgr A* being in a binary with a $\sim 10^2 - 10^4\,M_\odot$ *intermediate mass black hole* (IMBH) persists (cf. GRAVITY Collaboration et al. 2020, appendix 4). In the present day Universe, such IMBHs are thought to be formed in stellar cluster cores via hierarchical mergers of existing black holes (Miller & Hamilton 2002; Antonini, Gieles & Gualandris 2019; Rizzuto et al. 2022; Fragione et al. 2022a) or repeated mergers of main sequence stars to form a single massive star which then collapses to an IMBH seed (Portegies Zwart & McMillan 2002; Gürkan, Freitag & Rasio 2004; González et al. 2021; Ballone et al. 2023). These clusters can then be driven towards the centres of galaxies by dynamical friction and their IMBHs deposited in the vicinity of a SMBH (Tremaine, Ostriker & Spitzer 1975; Mastrobuono-Battisti, Perets & Loeb 2014; Arca-Sedda & Gualandris 2018; Fragione 2022). Alternatively, IMBHs can form and grow directly in the nuclear star clusters (NSC) of galaxies via accretion from an AGN disc (McKernan et al. 2012, 2014) or by repeated mergers with black holes and stars (Stone, Küpper & Ostriker 2017; Rose et al. 2022; Fragione et al. 2022b; Atallah et al. 2023). Observational searches for IMBHs and theoretical explorations of their formation and growth mechanisms have been widely discussed in recent years—see Greene, Strader & Ho (2020) for a review.

★ E-mail: fraser.evans@utoronto.ca

It is conceivable, then, that Sgr A* has a dark companion which, owing to the fact that the GC makes for a challenging observational environment (see Schödel et al. 2014, for a review), has not yet been detected. A consequence of such a massive black hole binary (MBHB) existing in the GC is that close dynamical interactions between single stars and the MBHB would tend to 'fling' the stars out at roughly the orbital velocity of the less massive member of the MBHB, draining energy from the binary system (Quinlan 1996; Zier & Biermann 2001). Ejection velocities increase as the MBHB hardens, to the point where a tight MBHB is able to eject so-called 'hypervelocity stars' (HVSs) with velocities in excess of the Galactic escape speed (Yu & Tremaine 2003). Note that a companion to Sgr A* is not required to produce HVSs—the term HVS was coined by Hills (1988), who first theorized that the disruption of a stellar binary by a single SMBH could eject one member of the binary with an extreme velocity (see also Kenyon et al. 2008; Sari, Kobayashi & Rossi 2010; Kobayashi et al. 2012; Rossi, Kobayashi & Sari 2014; Generozov & Madigan 2020; Generozov 2021). While this 'Hills mechanism' remains the most promising scenario for the ejection of fast stars from the centre of the Galaxy, the 'MBHB slingshot' mechanism described above is a well-researched alternative (Levin & Beloborodov 2003; Baumgardt, Gualandris & Portegies Zwart 2006; Sesana, Haardt & Madau 2006, 2007a; Löckmann, Baumgardt & Kroupa 2008; Marchetti et al. 2018; Darbha et al. 2019; Rasskazov et al. 2019; Zheng, Lin & Mao 2021; Mastrobuono-Battisti et al. 2023).

Since the first detection of a promising HVS candidate by Brown et al. (2005), other candidate stars potentially unbound to the Galaxy have trickled in courtesy of targeted surveys (Brown et al. 2006; Brown, Geller & Kenyon 2009a, 2012, 2014), follow-up observations of previously identified stars (e.g. Heber et al. 2008; Tillich et al. 2009; Irrgang et al. 2010, 2019) and queries of large Galactic surveys (e.g. Palladino et al. 2014; Zhong et al. 2014; Huang et al. 2017; Koposov et al. 2020). See Brown (2015) for a review of these objects. While the current roster of proposed HVS candidates stands at ∼two dozen, only S5-HVS1 (Koposov et al. 2020) can be uncontroversially associated with an origin in the GC.

In its third and most recent data release (DR3), the European Space Agency satellite *Gaia* (Gaia Collaboration et al. 2016, 2022), measures five-parameter astrometry (parallax, position, and proper motion) and heliocentric radial velocities for ∼34 million sources (Gaia Collaboration et al. 2022; Katz et al. 2022; Sartoretti et al. 2022). Since its launch, *Gaia* observations have been invaluable in the identification of new potential HVS candidates (Bromley et al. 2018; Hattori et al. 2018; Li et al. 2018, 2021, 2022; Shen et al. 2018; Du et al. 2019; Luna, Minniti & Alonso-García 2019; Huang et al. 2021; Prudil et al. 2022; El-Badry et al. 2023; Igoshev, Perets & Hallakoun 2023). However, currently missing from all data releases of *Gaia* radial velocity catalogues are high-confidence HVS candidates, that is, candidates with (i) a precise astrometric solution (relative parallax error <20 per cent), (ii) a velocity which suggests the star is unbound to the Galaxy, and (iii) a trajectory which is consistent with an origin in the GC (Marchetti, Rossi & Brown 2019; Marchetti 2021; Marchetti, Evans & Rossi 2022).

This presents a tantalizing opportunity. If Sgr A* has a hidden companion, HVSs ejected via the MBHB slingshot mechanism may be detectable by *Gaia*. Given that the selection functions of both the *Gaia* astrometric catalogue and radial velocity catalogue are relatively well-modelled (Cantat-Gaudin et al. 2022; Everall & Boubert 2022; Castro-Ginard et al. 2023), it is possible to determine with reasonable confidence which stars should appear in the catalogue and which stars should not. In this work, we simulate populations of HVSs ejected from a MBHB located in the GC. Using these simulations, we can constrain the mass of a hidden companion to Sgr A* and its separation from Sgr A* by identifying MBHB configurations, which predict an abundance of confident HVS detections in the *Gaia* DR3 radial velocity catalogue. This work is a companion to Evans, Marchetti & Rossi (2022a, b) and Marchetti et al. (2022), in which we followed a similar philosophy focusing on the Hills mechanism. In these works, we showed that the lack of confident HVS detections in *Gaia* and the existence of S5-HVS1 constrains the ejection rate of HVSs via the Hills mechanism and the shape of the initial mass function (IMF) among HVS progenitor binaries.

This paper is organized as follows. In Section 2, we outline on a step-by-step basis our model for generating mock populations of HVSs ejected via the MBHB slingshot mechanism. In Section 3, we present our analyses of these populations—we show how the population of HVSs in *Gaia* depends on the characteristics of the MBHB binary and how the *absence* of high-confidence HVS candidates in *Gaia* DR3 constrains the mass of an as-of-yet unseen companion to Sgr A* and its separation from it. We discuss these results in Section 4, before offering a summary and conclusions in Section 5.

2 MBHB SLINGSHOT EJECTION MODEL

In this section, we describe how we model the MBHB orbital evolution, how we generate ejected HVSs, how we propagate these HVSs through the Galaxy, and how we obtain mock observations of them to determine, which would be detectable by *Gaia*. Overall our procedure resembles the approach of Marchetti et al. (2018), who also explore *Gaia*-detectable HVSs ejected from an MBHB in the GC. We expand upon their modelling by investigating a larger set of MBHB configurations and by using updated prescriptions for propagating HVSs through the Galaxy, performing mock photometry, and modelling the *Gaia* selection function. The code we use to implement the model we describe in this section is included as the `MBHB` module in the publicly available `PYTHON` package `speedystar`.[1]

2.1 Orbital decay of the MBHB

An MBHB embedded in a collisionless, fixed stellar background loses orbital energy via (i) the ejection of stars via the MBHB slingshot mechanism, and (ii) the emission of gravitational waves. We model the hardening of the MBHB during phase (i) following Quinlan (1996):

$$\left.\frac{da}{dt}\right|_{\rm HVS} = -\frac{G\rho H}{\sigma}a^2\,, \tag{1}$$

where G is the gravitational constant, ρ and σ are the mass density and one-dimensional velocity dispersion of the stellar background, respectively, assumed here to be $\rho = 7\times10^4\,{\rm M}_\odot\,{\rm pc}^{-3}$ (Schödel et al. 2007, 2014; Feldmeier et al. 2014) and $\sigma = 100\,{\rm km\,s}^{-1}$ (Figer et al. 2003; Schödel, Merritt & Eckart 2009; Feldmeier et al. 2014; Do et al. 2020) and H is a dimensionless hardening rate:

$$H(\sigma,\rho,a) = \frac{\sigma}{G\rho}\frac{d}{dt}\left(\frac{1}{a}\right)\,. \tag{2}$$

H must be computed from scattering experiments. When the binary separation is smaller than the hardening separation $a_{\rm h}$, H is approximately constant and typically in the range $15 \lesssim H \lesssim 20$ depending

[1] https://github.com/fraserevans/speedystar

on the binary mass ratio and eccentricity (Quinlan 1996; Sesana et al. 2006; Rasskazov et al. 2019). $a_{\rm h}$ is defined as

$$a_h \equiv \frac{GM_{\rm c}}{4\sigma^2}\,, \tag{3}$$

where $M_{\rm c}$ is the mass of the less-massive companion in the MBHB.

We approximate the orbital decay of the MBHB due to gravitational wave emission following Peters (1964):

$$\left.\frac{da}{dt}\right|_{\rm GW} = -\frac{64}{5}G^3c^5\frac{M_{\rm SgrA^*}M_{\rm c}M_{\rm total}}{a^3}\,, \tag{4}$$

where c is the speed of light, $M_{\rm SgrA^*}$ is the mass of Sgr A*, taken here as $4\times10^6\,{\rm M}_\odot$ (Eisenhauer et al. 2005; Ghez et al. 2008), and $M_{\rm total}\equiv M_{\rm SgrA^*}+M_{\rm c}$ is the total mass of the MBHB. The evolution of the MBHB semimajor axis with time is then

$$a(t) = a_0 + \int_{t_0}^{t}\left(\left.\frac{da}{dt}\right|_{\rm HVS} + \left.\frac{da}{dt}\right|_{\rm GW}\right)dt\,, \tag{5}$$

where at an initial time t_0 the binary starts at separation $a=a_0$.

Following as well from Quinlan (1996), the total mass $\Delta M_{\rm ej}$ in stars ejected by the MBHB as it shrinks from separation a to $a-\Delta a$ is modelled using the dimensionless mass ejection rate J:

$$\Delta M_{\rm ej} = J M_{\rm total}\Delta\ln(1/a)\,. \tag{6}$$

Note that this ejection rate above assumes the MBHB orbital decay is driven *entirely* by HVS ejections. To account for the contribution of GW emission to the binary hardening, we must include a correction to equation (6):

$$\Delta M_{\rm ej} = \frac{\Delta t_{\rm HVS}^{-1}}{\Delta t_{\rm total}^{-1}} J M_{\rm total}\Delta\ln(1/a)\,, \tag{7}$$

where $\Delta t_{\rm total}$ is the total time required for the MBHB to shrink from separation a to $a-\Delta a$ and $\Delta t_{\rm HVS} > \Delta t_{\rm total}$ is the time required to shrink from a to $a-\Delta a$ if the decay is entirely due to HVS ejections, calculated by integrating and inverting equation (1).

Over a grid of MBHB mass ratios q in the range $3\times10^{-5}\leq q\leq10^0$, we determine the dimensionless hardening rate H and the mass ejection rate J by perform scattering experiments. The methodology of these experiments closely follows Rasskazov et al. (2019) and we refer the reader to that work for more details. Stars, assumed to be massless, approach a MBHB of separation a from infinity with a velocity v, impact parameter b, from a direction drawn randomly with respect to the binary phase and orbital plane. v is drawn from a Maxwellian distribution in the range $[3\times10^3 v_0\sqrt{q/(1+q)}, 30v_0\sqrt{q/(1+q)}]$ (Sesana et al. 2006), where

$$v_0 \equiv \sqrt{\frac{G(M_{\rm c}+M_{\rm MBH})}{a}} \tag{8}$$

is the orbital velocity of the MBHB. b^2 is drawn uniformly such that pericentre distances are constrained to the range $[0, 5a]$. We assume the scattering interactions never increase the eccentricity of the binary—its orbit remains circular throughout (see discussion on this point in Section 4). Each star is scattered off the MBHB and the simulation ends when (i) the star reaches a distance of $50a$ from the MBHB with a positive total energy, or (ii) the time-scale for the scattering interaction exceeds 10 Gyr, or (iii) when the star spends longer than 1.6×10^4 binary orbital periods within a distance of $50a$ from the MBHB. For each mass ratio q we run a total of four million such simulations using the ARCHAIN (Mikkola & Merritt 2008) algorithm, specifically developed to simulate small-N systems.

The results of these simulations are shown in Fig. 1, where we plot how H and J depend on the MBHB separation for various mass ratios. In our calculation of J, a star counts as 'ejected' if and only if its velocity at a large distance from the MBHB is larger than $5.5\sigma = 550\,{\rm km\,s^{-1}}$, which is approximately the escape velocity from the bulge if it is modelled as a single isothermal sphere profile. In general, H at fixed $a/a_{\rm h}$ increases with decreasing q though the relationship is not strictly monotonic. Note as well that more massive binaries still merge more quickly since $a_{\rm h}$ decreases linearly with q. In agreement with Sesana et al. (2006), we find that each can be approximated as

$$H(a) = A_H(1+a/a_{0,H})^{\gamma_H}\,, \tag{9}$$

$$J(a) = A_J(a/a_{0,J})^{\alpha_J}(1+(a/a_{0,J})^{\beta_J})^{\gamma_J}\,, \tag{10}$$

where A, α, β, and γ are fitting parameters. In Table 1, we share best-fitting parameters for a selection of mass ratios.

Another result of our scattering experiments, echoing the results of Rasskazov et al. (2019), is that the high-velocity tail of the ejection velocity distribution ($v_{\rm ej}\geq400\,{\rm km\,s^{-1}}$) is well-fit by a broken power-law distribution of the form

$$\frac{{\rm dN}}{{\rm dlog}v_{\rm ej}} = \begin{cases} C_1, & \text{if } v_{\rm ej} < v_{\rm break} \\ C_2 v_{\rm ej}^{-3.1}, & \text{if } v_{\rm ej}\geq v_{\rm break}\end{cases}\,, \tag{11}$$

where C_1 and C_2 are constants, $v_{\rm break}=1.2v_0\sqrt{2q}/(1+q)$ and v_0 is the circular velocity of the MBHB (equation (8)). When assigning initial velocities to ejected stars, we draw velocities at random from this distribution in the range $[5.5\sigma, 5v_0]$.

In Fig. 2, we summarize our modelling of the MBHB orbit, showing the orbital decay and the stellar mass ejection rate for $q=10^{-1}$, $q=10^{-2}$, and $q=10^{-3}$. Each binary has an initial separation of $a_0=100\,{\rm pc}$ at $t=0$, and for the purposes of this study it is sufficient to say the MBHB has 'merged' when its separation reaches $10^{-6}\,{\rm pc}$, as after this the separation will drop to zero within a year. The top panel shows the elapsed time required for the MBHB to shrink to a separation a. The total time to merge is quite sensitive to the companion mass—the $q=10^{-1}$, $q=10^{-2}$, and $q=10^{-3}$ binaries merge within 36.5 Myr, 60 Myr, and 151 Myr, respectively. The vertical lines show the hardening separations $a_{\rm h}$ for the corresponding mass ratio. The MBHB reaches $a=a_{\rm h}$ at earlier stages of the inspiral for progressively more massive companions. The middle panel shows that the HVS mass ejection rate profile peaks shortly after $a=a_{\rm h}$. For small q, this peak occurs after $da/dt|_{\rm HVS}=da/dt|_{\rm GW}$ (see bottom panel) and as q increases this peak occurs while the slingshot mechanism is still the dominant hardening mechanism. The total ejected HVS mass also depends strongly and non-linearly on the MBHB companion mass—a binary with a mass ratio of 10^{-2} ejects 152 times more HVS mass in total than a binary with a mass ratio of 10^{-4}, but only eight times more mass than a binary with a mass ratio of 10^{-3}.

2.2 Generating the HVS sample

The previous subsection described how the mass ejected in HVSs by a MBHB is related to the characteristics and evolution of the binary. Here, we describe how we apply this to generate individual mock HVSs. Our approach is as follows.

We assume a MBHB composed of Sgr A* and a companion of mass $M_{\rm c}$ started initially at separation $a_0=100\,{\rm pc}$ at time t_0 and is now at separation $a_{\rm now}$. We create a grid of 1000 semimajor axes from $a_{\rm now}$ to a_0 uniformly spaced in log-space. This large initial separation ensures we capture all HVS ejections. In practice, we find

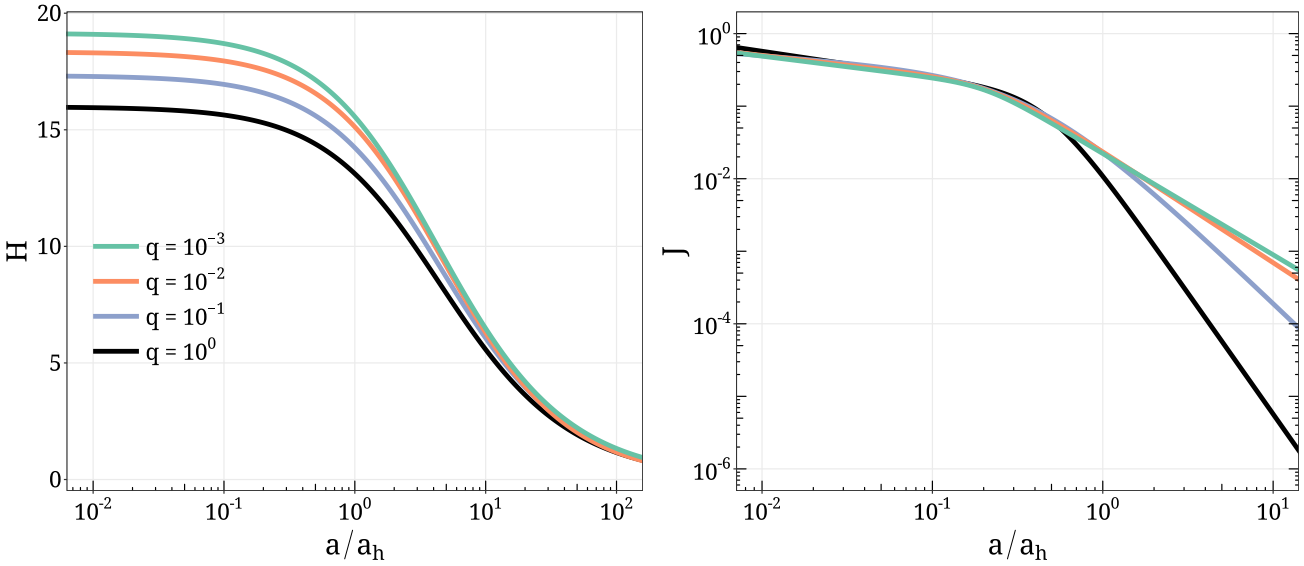

Figure 1. The dependence of the dimensionless hardening rate H (left-hand panel) and mass ejection rate J (right-hand panel) on the MBHB hardness, assuming a circular MBHB orbit. MBHB separations are scaled to the hardening separation (equation (3)) Relationships for MBHBs with differing mass ratios (q) are shown with different line colours.

Table 1. Best-fitting parameters for the hardening rate H and stellar mass ejection rate J (see equation (9)).

Mass ratio	A_H	$a_{0,H}/a_h$	γ_H	A_J	$a_{0,J}/a_h$	α_J	β_J	γ_J
1.0	14.58	1.98	−0.62	0.21	0.14	−0.36	11.17	−0.20
0.3	15.98	3.42	−0.77	0.15	0.48	−0.35	2.77	−1.08
0.1	17.33	3.43	−0.77	0.26	0.41	−0.18	1.32	−1.57
0.03	18.34	3.86	−0.84	0.22	0.24	−0.27	2.37	−0.54
0.01	19.14	3.24	−0.77	0.20	0.21	−0.29	3.75	−0.29
0.003	18.27	4.00	−0.81	0.21	0.20	−0.30	4.31	−0.26
0.001	17.29	3.29	−0.75	0.22	0.21	−0.30	3.93	−0.30
0.0003	17.36	2.92	−0.73	0.22	0.22	−0.29	3.46	−0.36

that the ejection rate of fast stars from the MBHBs we explore is negligible for $a \lesssim 0.1$ pc and only stars ejected when the MBHB is at a separation of $\lesssim 0.1$ pc are detectable in any *Gaia* data release.

We use equation (7) to determine the mass $\Delta M_{\mathrm{ej},i}$ ejected while the binary was in the ith separation bin, $i = 1, 2, ..., 1000$. The corresponding *number* of ejected HVSs is

$$\Delta N_i = \frac{\Delta M_{\mathrm{ej},i}}{\int_{M_{\mathrm{min}}}^{M_{\mathrm{max}}} M f(M) dM} , \tag{12}$$

where $f(M)$ is the assumed IMF, defined between minimum and maximum stellar masses M_{min} and M_{max}. We adopt a single power-law IMF with slope κ, i.e. $f(m) \propto m^{-\kappa}$ and minimum and maximum masses of $0.1\,\mathrm{M}_\odot$ and $100\,\mathrm{M}_\odot$, respectively.

If the MBHB is currently at separation a_{now}, the flight time of all stars ejected while the binary was in the ith separation bin have the same flight time $t_{\mathrm{flight},i}$:

$$t_{\mathrm{flight},i} = \int_{a_i}^{a_{\mathrm{now}}} \left(\left.\frac{da}{dt}\right|_{\mathrm{HVS}} + \left.\frac{da}{dt}\right|_{\mathrm{GW}} \right)^{-1} da , \tag{13}$$

where a_i is the mid-point of the ith separation bin. We assume a star is equally likely to be ejected at any point in its lifetime, therefore we say the age of each star at ejection $t_{\mathrm{age,ej}}$ is a random fraction of its maximum lifetime t_{life};

$$t_{\mathrm{age,ej}} = \epsilon \cdot t_{\mathrm{life}} , \tag{14}$$

where ϵ is a random number uniformly distributed in [0,1]. t_{life} for each ejected star is determined using the single stellar evolution (SSE; Hurley, Pols & Tout 2000) algorithms within the AMUSE[2] environment (Portegies Zwart et al. 2009, 2013; Pelupessy et al. 2013; Portegies Zwart & McMillan 2018), taking the start of the asymptotic giant branch phase as the 'end' of a star's life. We cap t_{life} to a maximum of 13.8 Gyr to ensure the star is not older than the Universe.

Today, the age of each star is

$$t_{\mathrm{age}} = t_{\mathrm{age,ej}} + t_{\mathrm{flight}} . \tag{15}$$

We remove stars for whom $t_{\mathrm{age}} > t_{\mathrm{life}}$, i.e. stars, which were ejected as main sequence or evolved stars but are stellar remnants in the present day.

After drawing an ejection velocity for each surviving star following equation (11), stars are initialized on a sphere 3 pc in radius centred on Sgr A* with a velocity pointing radially away from the GC. This

[2] https://amuse.readthedocs.io/en/latest/index.html

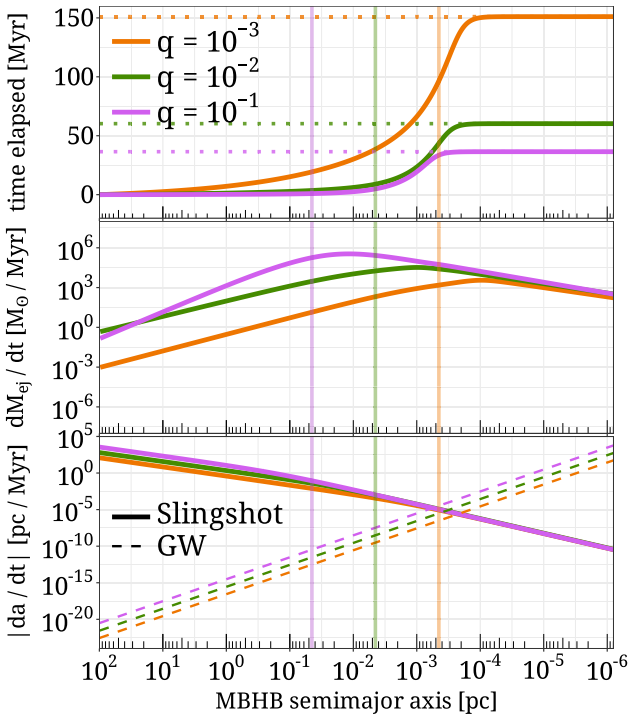

Figure 2. The MBHB orbital decay and rate of mass in ejected stars as a function of binary semimajor axis, for three values of the mass ratio q. The coloured vertical lines show the hardening separation (equation (3)) for the corresponding mass ratio. The primary MBH mass in each scenario is assumed to be $4 \times 10^6\,\mathrm{M}_\odot$ and each starts at $t = 0$ at a separation $a_0 = 100\,\mathrm{pc}$. The top panel shows how the separation shrinks with time, with the dotted horizontal lines showing when each binary merges. The middle panel shows how the stellar mass ejection rate evolves throughout the inspiral. The bottom panel shows how the decay rate changes with decreasing separation, with the contributions from HVS ejections and from GW emissions plotted separately.

is roughly We assume stars are ejected isotropically—we comment further on this assumption in Section 4.

2.3 Orbital integration and mock photometry

After initializing our mock HVSs, our scheme for propagating them forward in time through the Galactic potential and obtaining synthetic photometry of them remains essentially unchanged from the method described in Evans, Marchetti & Rossi (2022b). We refer the reader to that work for more detailed explanations and briefly summarize the approaches here.

We propagate each star forward in time for its flight time assuming the Galactic potentials of McMillan (2017), who use a Monte Carlo Markov Chain (MCMC) method to fit a many-component potential to various kinematic data. For each realization, we draw a potential at random from the McMillan (2017) MC chain (McMillan, private communication). All ejected stars are integrated through this potential with the `PYTHON` package `GALPY`[3] (Bovy 2015) using a fifth-order Dormand–Prince integrator (Dormand & Prince 1980) and a timestep of 0.1 Myr.

We estimate the visual dust extinction at each star's distance and sky position using the COMBINED15 dust map of (Bovy et al. 2016),[4] itself a combination of the Galactic dust maps of Drimmel, Cabrera-Lavers & López-Corredoira (2003), Marshall et al. (2006), and Green et al. (2015). We then determine mock apparent magnitudes for each mock HVS in the photometric bands using the MESA Isochrone and Stellar Tracks, or `MIST` (Choi et al. 2016; Dotter 2016) models.[5] With each star's luminosity, surface gravity and effective temperature (determined with `AMUSE` depending on each star's mass, age, and metallicity), as well as its visual extinction, we interpolate the `MIST` bolometric correction tables to determine each star's apparent magnitude in the Johnsons–Cousins V and I_c bands (Bessell 1990) and *Gaia* G and G_{RP}, bands[6] (Riello et al. 2021). We estimate each star's magnitude in the *Gaia* G_{RVS} band from its V, I_c, and G-band magnitudes using fits from Jordi et al. (2010).

2.4 HVSs identifiable by *Gaia*

With mock magnitudes and stellar parameters for our synthetic HVS populations, we now determine which HVS candidates should be detectable in the different *Gaia* data releases with measured radial velocities. While we use an updated selection function, this approach is similar in philosophy to Evans et al. (2022b).

For *Gaia* DR3, we start by discarding all HVSs with effective temperatures outside the range $3500\,\mathrm{K} \leq T_{\mathrm{eff}} \leq 6900\,\mathrm{K}$, since the *Gaia* spectroscopic pipeline does not assign validated radial velocities to stars outside this temperature range (Katz et al. 2022; Sartoretti et al. 2022). Next, we use the selection functions made available by the GaiaUnlimited[7] project (Cantat-Gaudin et al. 2022; Castro-Ginard et al. 2023) to identify stars, which would be detectable in the *Gaia* DR3 radial velocity catalogue. In short, the DR3 empirical selection function is calibrated against the Dark Energy Camera Plane Survey Data Release 1 (Schlafly et al. 2018), and querying it yields the probability p_{source} that a star at a given sky position with a given *Gaia* G-band magnitude would appear in the DR3 source catalogue, i.e. it would have at least a measured position, magnitude and colour. Since it compares to a deeper survey, We note that this approach only characterizes the faint-end selection function of *Gaia*. At the bright end, saturation effects lead to incompleteness for sources brighter than $G \lesssim 3$ (see Fabricius et al. 2021; Gaia Collaboration et al. 2021). We remove all mock HVSs brighter than $G = 3$, however, we note that it is extraordinarily rare for our model to produce HVSs this bright. Likewise, querying the spectroscopic selection function yields the probability p_{vrad} that a star in the DR3 source catalogue at a given sky position, G-band magnitude and $G{-}G_{\mathrm{RP}}$ colour is in the radial velocity catalogue as well. We manually set p_{vrad} to zero for mock HVSs in sky position/magnitude/colour bins entirely unpopulated in the DR3 radial velocity catalogue, since in the GaiaUnlimited statistical model p_{vrad} will be non-zero but small and highly uncertain. The total probability p that a mock HVS would appear in the *Gaia* DR3 radial velocity subsample is then the product of p_{source} and p_{vrad}. For each mock HVS in our sample we draw a uniform random number $0 < \epsilon < 1$ and designate the HVS as DR3-detectable if $\epsilon < p$.

After deciding which mock HVSs would have radial velocities in DR3, we determine each one's five-dimensional astrometric covariance matrix (position, parallax, and proper motion uncertainties and correlations amongst them) by querying the *Gaia* DR3

[3] https://github.com/jobovy/galpy
[4] https://github.com/jobovy/mwdust
[5] https://waps.cfa.harvard.edu/MIST/
[6] see https://www.cosmos.esa.int/web/gaia/edr3-passbands
[7] https://github.com/gaia-unlimited/gaiaunlimited

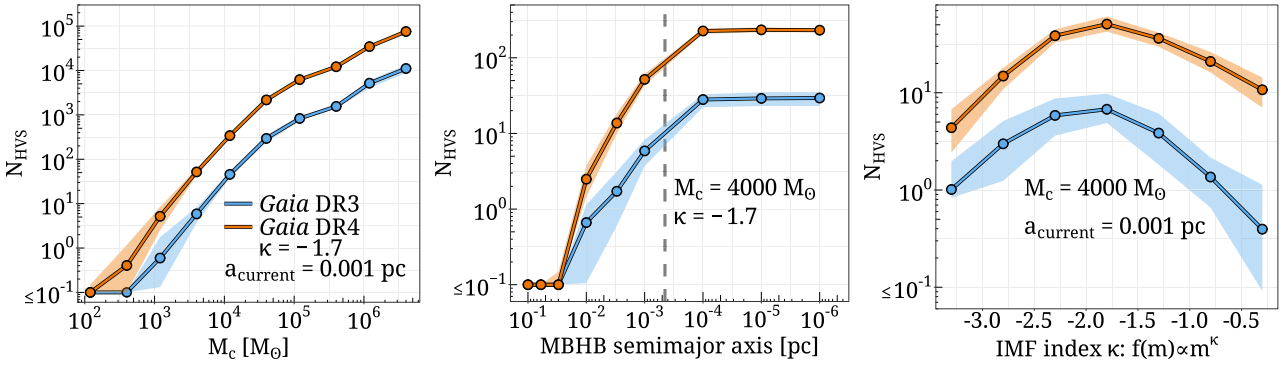

Figure 3. The population of high-confidence HVSs (see Section 2.4) expected to appear in *Gaia* DR3 and DR4. Panels show how N_{HVS} depends on the mass of the companion (left-hand panel), the current separation $a_{current}$ between Sgr A* and its companion (middle), and the slope κ of and IMF among HVS progenitors (right-hand panel). Parameters are fixed to their fiducial values when not being varied. Shaded regions span the 16th–84th quantiles over 40 iterations. The vertical dashed line in the middle panel shows the hardening separation for this binary.

astrometric spread function of Everall et al. (2021),[8] which computes uncertainties based on the sky position and *G*-band magnitude of the source. Finally, we determine the DR3 radial velocity uncertainty for each star using the `PYTHON` package `PyGaia`.[9]

We also determine which stars will be detectable in the fourth *Gaia* data release (DR4). Radial velocity measurements in this survey would be available for all mock HVSs cooler than 6900 K and brighter than the $G_{RVS} = 16.2$ mag faint-end magnitude limit of the *Gaia* radial velocity spectrometer (Cropper et al. 2018; Katz et al. 2019). For hotter HVSs, radial velocities would be available for stars brighter than $G_{RVS} = 14$. We estimate DR4 astrometric errors using Everall et al. (2021) DR3 astrometric spread function, reducing the errors according to the predicted *Gaia* performance.[10]

To be labelled as a 'detectable' high-confidence HVS in a particular *Gaia* DR3 or DR4, an ejected star must:

(i) Be brighter than the faint-end apparent magnitude limit of the radial velocity catalogue of the data release.
(ii) Have an effective temperature range within the bounds imposed by each data release (see above).
(iii) Have a relative parallax uncertainty below 20 per cent. For larger uncertainties, estimating distances (and therefore total velocities) becomes problematic (see Bailer-Jones 2015).
(iv) Have a total velocity in the Galactocentric rest frame in excess of 700 km s^{-1}. We sample over the astrometric and radial velocity uncertainties of each mock star and compute its total velocity assuming a distance from the Sun to the GC of 8.122 kpc (GRAVITY Collaboration et al. 2018), a height of the Sun above the Galactic disc of 20.8 pc (Bennett & Bovy 2019) and a rest-frame velocity of the Sun of $\mathbf{v}_\odot \equiv [U_\odot, V_\odot, W_\odot] = [12.9, 245.6, 7.78]$ km s^{-1} (Reid & Brunthaler 2004; Drimmel & Poggio 2018). Upon sampling, in at least 80 per cent of realizations the total velocity of the star must be above 700 km s^{-1}.

These above cuts resemble those used to search for HVS candidates in *Gaia* Data Release 2 (Marchetti et al. 2019), Early Data Release 3 (Marchetti 2021) and DR3 (Marchetti et al. 2022). We remark that Marchetti et al. (2019), Marchetti (2021), and Evans et al. (2022a, b) selected HVSs by searching for stars likely to be moving faster than the Galactic escape speed at their position. In Marchetti et al. (2022) and in this work, however, we focus instead on stars moving faster than 700 km s^{-1}. Determining the boundedness of a star requires assuming a Galactic potential, whereas a single velocity cut instead allows agnosticism towards the potential. This cut at 700 km s^{-1} is conservative—in reasonable models of the Milky Way potential the escape velocity is <700 km s^{-1} everywhere except perhaps the within the innermost kpc of the Galaxy in heavier models (e.g. McMillan 2017).

For brevity, in the remainder of this work we use the terms '*Gaia* DR3/DR4' to refer exclusively to the radial velocity subsamples, and by the term 'HVS' we refer only to those stars, which satisfy the criteria listed above.

3 RESULTS

3.1 An existing companion to Sgr A*

Having outlined our model for generating mock HVS populations from the MBHB slingshot mechanism, we start in Fig. 3 by illustrating how the HVS population detectable in *Gaia* DR3 and DR4 depends on our model assumptions. In the left-hand panel, we show how the *Gaia* HVS population depends on the IMBH companion mass when the MBHB separation is fixed at 1 mpc and the IMF of HVS progenitors has a power-law slope of −1.7 (Lu et al. 2013). Below a companion mass of $\simeq 600\,M_\odot$, we expect ≤1 HVS in both DR3 and DR4. This expected DR3 population can rise to several tens of thousands if Sgr A* is in a near-equal mass MBHB. The steep dependence on M_c is fairly intuitive—as the companion mass increases, the total ejected stellar mass increases and the ejection velocity distribution shifts towards higher velocities (Fig. 2, equation (11)). A strong dependence on the current separation $a_{current}$ of the MBHB (middle panel) is digestible as well—a smaller current separation means the MBHB has ejected more HVSs in the recent past, and HVS ejection velocities are larger since the MBHB circular velocity is larger. N_{HVS} plateaus for separations smaller than the binary hardening separation (vertical line) because the binary merges shortly thereafter (see Fig. 2). For an HVS IMF slope of −1.7 and a companion mass of $4000\,M_\odot$, >1 HVS is expected in *Gaia* DR3 as long as the MBHB separation is less than a few milliparsecs. This number should reach ∼60 in DR3 or several

[8] see https://github.com/gaiaverse/scanninglaw
[9] https://github.com/agabrown/PyGaia
[10] https://www.cosmos.esa.int/web/gaia/science-performance, see also Brown (2019).

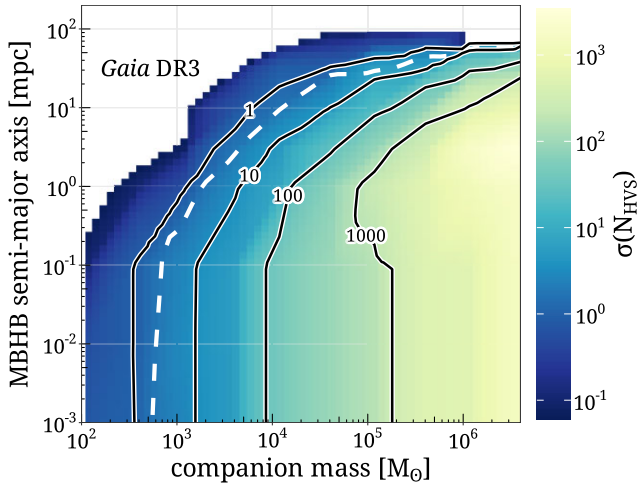

Figure 4. Contour lines show how the population of HVSs detectable in Gaia DR3 depends on the Sgr A* companion mass M_c and the current separation $a_{current}$ between Sgr A* and its companion, averaged over 40 realizations and smoothed over the grid. The colourbar shows the 1σ scatter of N_{HVS}. The white dashed line shows where the 1σ lower bound of N_{HVS} reaches one—the parameter space *above* this line is consistent with zero HVS detections in *Gaia* DR3.

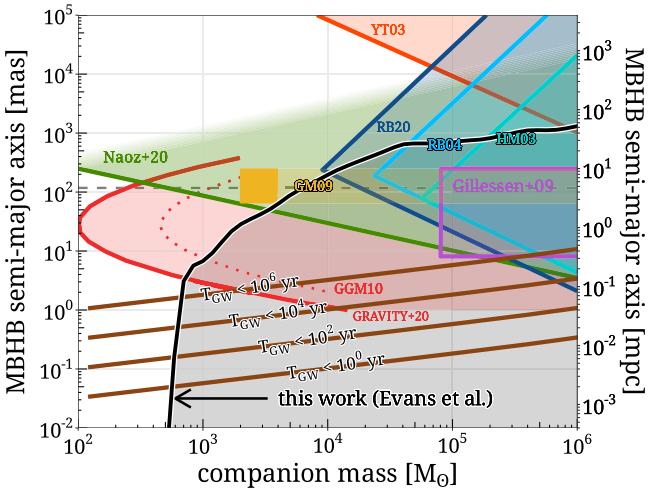

Figure 5. Constraints on the mass of a black hole companion to Sgr A* and its separation from Sgr A* in angle (left-hand axis) and physical space (right-hand axis). Adapted from GRAVITY Collaboration et al. (2020), adapted in turn from Gualandris & Merritt (2009). The lack of confident HVS candidates in *Gaia* DR3 excludes the region below the black line. The dashed horizontal line highlights the semimajor axis of S2 at 125 mas (≈ 4.7 mpc; GRAVITY Collaboration et al. 2020). Yu & Tremaine (2003) previously excluded the orange region by remarking that the barycentre of a presumed MBHB in the GC cannot be significantly displaced from Sgr A*, otherwise the cusp of stellar density in the GC would not be coincident with Sgr A*. The cyan, blue, and dark blue regions are excluded from astrometric observations of Sgr A* (Hansen & Milosavljević 2003; Reid & Brunthaler 2004, 2020). The violet region is excluded by the orbit of S2 (Gillessen et al. 2009). The green region is excluded by Naoz et al. (2020) by requiring that the orbit of S2 is stable against perturbations by a Sgr A* companion (a fading colour denotes weakening constraints). The solid gold region is excluded by Gualandris & Merritt (2009) using the orbital eccentricity distribution of the S-star cluster. Companion masses to the right of the dotted red line are excluded by Gualandris et al. (2010) from the orbit of S2. Following the 2018 pericentric passage of S2, these constraints were improved by GRAVITY Collaboration et al. (2020). The diagonal dotted lines show lines of constant gravitational wave inspiral time for the MBHB.

hundred in DR4 if the MBHB is just about to merge within the next decade.[11]

In the right-hand panel of Fig. 3, we show the dependence of N_{HVS} on the IMF power law slope κ. The turnover at $\kappa \simeq -1.7$ can be explained by two competing factors. First, as κ increases, ejected stars are on average more massive, and therefore more luminous and more likely to be brighter than *Gaia*'s faint-end magnitude limit of ∼14 for the DR3 radial velocity sample. Secondly, however, the total number of ejected HVSs *decreases* as κ increases, since the ejected stellar mass is locked up in fewer, more massive stars (see equation (7)). The turnover represents the point where the latter effect overcomes the former.

Since the impact of κ on N_{HVS} in DR3 is comparatively weak (particularly in the vicinity of $\kappa \approx -1.7$), for the remainder of this work we explore only constraints on $a_{current}$ and M_c. We run simulations over a $M_c/a_{current}$ grid, marginalizing over κ by sampling it at random in each iteration from a Gaussian distribution centred on $\kappa = -1.7$ with a standard deviation of 0.2 (Lu et al. 2013). In Fig. 4, we show the results of this simulation suite. The contours show lines of constant N_{HVS} throughout $M_c - a_{current}$ space and the colourbar indicates the 1σ scatter. For our fiducial choices of $M_c = 4000\,M_\odot$ and $a_{current} = 1$ mpc, we determine that 6 ± 3 high-confidence HVSs should have been uncovered in the radial velocity catalogue of *Gaia* DR3. Following from Fig. 3, the expected DR3 HVS population ranges from <1 (for low-mass companions at large separations) to ∼thousands (for a near-equal-mass, hardened MBHB). The relative scatter is $\sigma(N_{HVS})/N_{HVS} \simeq 0.2$ for $N_{HVS} \gtrsim 100$, rising to ≃0.5 and ≃1 if ∼tens or only a few HVS were uncovered, respectively. For $M_c \lesssim 10^5\,M_\odot$ N_{HVS} increases monotonically with decreasing $a_{current}$.

For larger companion masses, however, N_{HVS} decreases for $a_{current}$ less than ∼ a few × 10^{-1} mpc since the MBHB slingshot mass ejection rate peaks and begins to decline before GW emission takes over and the binary quickly merges (see Fig. 2 middle panel). The dashed white line indicates where the 1σ lower limit of N_{HVS} is equal to one, i.e. where one HVS *at least* should be in the survey. Since no such HVSs have been detected in *Gaia* DR3, MBHB binaries below this line can be excluded. A companion to Sgr A* cannot exist within 1 mpc (2000 AU) of the GC unless it is quite low-mass ($M_c \lesssim 2000\,M_\odot$). A near-equal mass MBHB remains possible only for separations $\gtrsim 0.05$pc.

Prior works have constrained a companion to Sgr A*. In Fig. 5, we place our constraints in context with these. In all, large regions of the parameter space we exclude in this work have previously been excluded, particularly cases where Sgr A* has a fairly massive companion just inside or outside the orbit of S2. These configurations, if true would result in an astrometric 'wobble' of Sgr A* (Hansen & Milosavljević 2003; Reid & Brunthaler 2004, 2020), would impact the orbit of S2 (Gillessen et al. 2009), its stability against perturbation (Gualandris, Gillessen & Merritt 2010; GRAVITY Collaboration et al. 2020; Naoz et al. 2020) and the stability of the S-star cluster in general (Gualandris & Merritt 2009). HVS observations are an independent tool to measure the GC and the constraints they impose

[11] A small point of possible confusion—for simplicity, we assume the MBHB separation does not shrink throughout the *Gaia* mission lifetime. Given typical MBHB coalescence times (see Fig. 2), this assumption is valid. The analysis presented in this work assumes a scenario in which *Gaia* DR3 and DR4 are 'snapshots' of the Milky Way at a time when the MBHB separation is $a_{current}$, rather than observations collected over the span of 34 or 66 months, respectively.

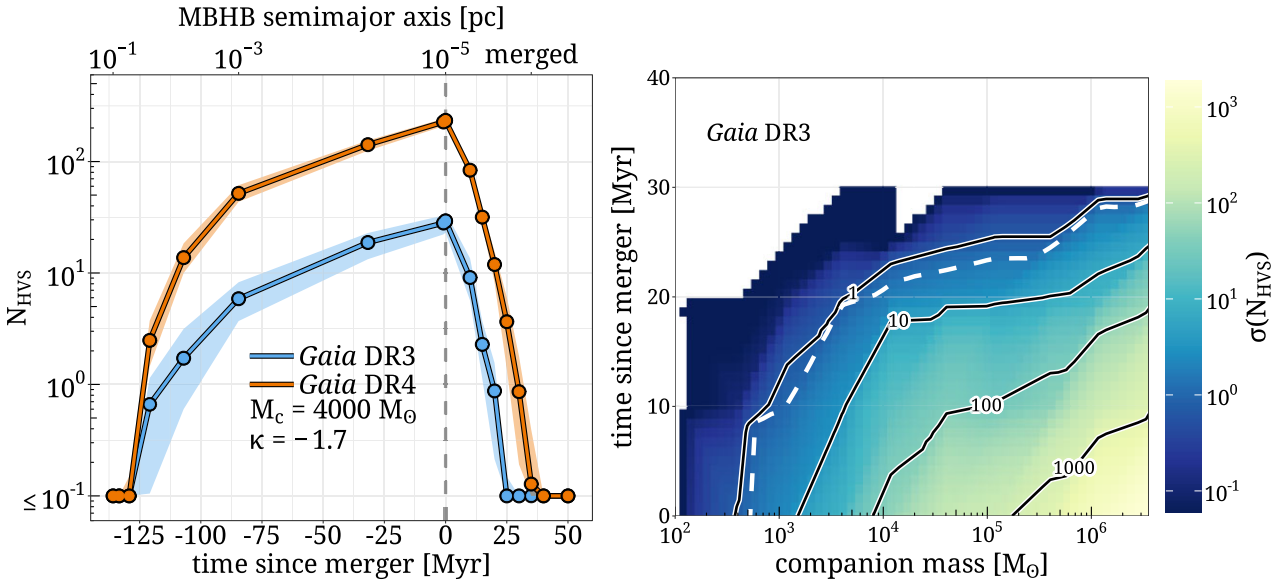

Figure 6. Left-hand panel: the dependence of $N_{\rm HVS}$ on the time $t_{\rm since}$ since the MBHB has merged with a companion. A negative $t_{\rm since}$ indicates that the MBHB has not yet merged—when this is the case, the top horizontal axis indicates the MBHB separation. Shaded regions span the 16th–84th quantiles over 50 iterations. Right-hand panel: contour lines show how the population HVSs detectable in Gaia DR3 depends on the former Sgr A* companion mass $M_{\rm c}$ and time elapsed since the merger $t_{\rm since}$, averaged over 20 realizations and smoothed over the grid. The colourbar shows how the 1σ scatter of $N_{\rm HVS}$. The dashed line shows where the 1σ lower bound of $N_{\rm HVS}$ equals one.

on a possible MBHB in the GC reinforce and somewhat sharpen these prior constraints. Some additional constraints exist, which for clarity have not been included in Fig. 5. GRAVITY Collaboration et al. (2023) use observations of S2 and employ dynamic nested sampling (see Speagle 2020) to constrain the presence of an IMBH within or just outside S2's orbit. They exclude IMBHs more massive than 2000 $M_\odot$ within 100 mas of the GC. For IMBHs in the separation range [100, 1000] mas the parameter space of possible solutions becomes quite chaotic, however, most of these solutions would result in the disruption of the S-star cluster within a million years. Tep et al. (2021) model the susceptibility of the S-star cluster eccentricities to diffusion from scalar resonant relaxation. Fouvry, José Bustamante-Rosell & Zimmerman (2023) similarly model how vector resonant relaxation impacts the orbital orientations of S-stars. Both works find generally that assuming the S-stars were born on an initially near-circular disc, the present-day orientations and eccentricities of these stars are incompatible with a significant population of $M \geq 100\,M_\odot$ IMBHs within 100 mpc of the GC.

Of the parameter space that has *not* already been excluded by previous works, we mainly rule out companions separated from Sgr A* by less than a milliparsec. Such configurations, depending on the mass of the companion, could only persist for a short amount of time between gravitational wave emission drives the MBHB to coalescence. We annotate Fig. 5 with lines of constant gravitational wave coalescence times. Some prior works have disregarded configurations below these lines outright, as it would be fortuitous if at present Sgr A* were about to merge with a companion in the very near future. Regardless, a lack of HVS candidates in *Gaia* DR3 observations exclude such fortunate scenarios and demonstrates the advantage of using HVS observations alongside other probes. Combining prior constraints with constraints determined in this work, the allowed configurations of a MBHB in the GC are limited to (i) a $\lesssim 5 \times 10^4\,M_\odot$ companion at a separation greater than a few tens of milliparsecs from Sgr A*, (ii) a $M = 100 - 200\,M_\odot$ companion just within or outside the orbit of S2 (970 AU, or 4.7 mpc), or (iii) a $M \lesssim 500 - 600\,M_\odot$ companion at a separation of less than a few hundred microparsecs from Sgr A*.

3.2 A *former* companion to Sgr A*

As the MBHB spirals in, the HVS mass ejection rate peaks at a small separation (Fig. 2, see also Gualandris, Portegies Zwart & Sipior 2005; Baumgardt et al. 2006; Levin 2006). Post-merger, this final 'gasp' of HVSs propagates outwards through the Galaxy. Over the next ∼tens of Myr, these HVSs can still be detected from Earth. This means HVS observations can probe not only an existing companion to Sgr A*, but a former companion as well. We illustrate this in Fig. 6. In the left-hand panel, we show how $N_{\rm HVS}$ depends on the time $t_{\rm since}$ since the MBHB in the GC merged, holding teh companion mass and IMF index fixed. A negative $t_{\rm since}$ indicates the binary has not yet merged. $N_{\rm HVS}$ is largest just before the MBHB coalesces. Otherwise, from the HVS population size alone one cannot determine whether the MBHB exists in the present day or whether it already merged in the recent past. Given a substantial population of HVS candidates, the distribution of flight times could discriminate between these two scenarios (see Section 4).

In the right-hand panel of Fig. 6, we show how $N_{\rm HVS}$ depends on both $M_{\rm c}$ and $t_{\rm since}$ when we sample over κ as before. The dashed line indicates where the 1σ lower limit of $N_{\rm HVS}$ reaches one. Any configuration below this line can be ruled out, since at least one HVS ejected before the MBHB merged should still be detectable in *Gaia* DR3. If Sgr A* ever had a companion more massive than 1000 $M_\odot$, it must have merged with Sgr A* more than 10 Myr ago. This lower limit on $t_{\rm since}$ increases with increasing companion mass. To our knowledge this is the first direct observational constraint on the specific merger history of Sgr A* within the last ∼tens of Myr. If Sgr A* merged with a companion more than ∼30 Myr ago, we cannot offer constraints on how massive that companion could have been. Similarly, if Sgr A* recently accreted a companion less massive than

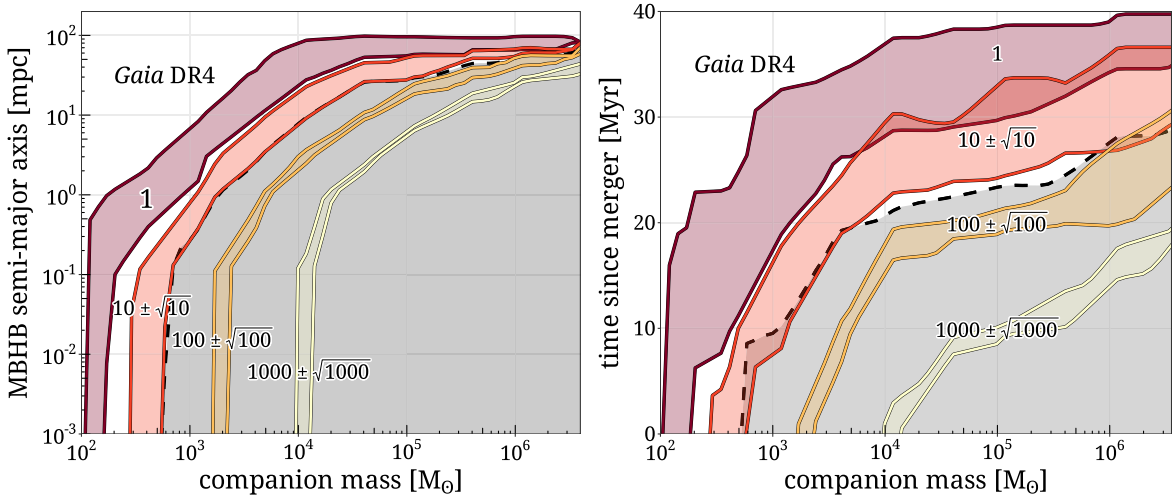

Figure 7. The coloured bands show configurations of M_c and $a_{current}$ (left-hand panel) or M_c and t_{since} (right-hand panel) space consistent within 1σ with finding the labelled number of HVSs in *Gaia* DR4. The shaded grey regions are already excluded by the lack of HVSs in *Gaia* DR3.

$\sim$500 $M_\odot$, current HVS observations cannot constrain how recently this merger occurred.

Sgr A*'s recent merger history is directly linked to the buildup of the Milky Way's NSC since any assumed IMBH would likely have been delivered to the GC by tidally disrupted star cluster which fell in (see Mastrobuono-Battisti et al. 2014; Arca-Sedda & Gualandris 2018; Askar, Davies & Church 2021; Fragione 2022). Constraints on Sgr A*'s most recent mergers then naturally lead to constraints on the most recent clusters accreted by the NSC. Our results suggest that within the last 10 Myr, Sgr A* has not merged with a companion more massive than 1000 $M_\odot$. Since a 1000 $M_\odot$ IMBH in a binary with Sgr A* takes 312 Myr to merge with Sgr A* from a separation of 10 pc, the inspiral of a cluster hosting Sgr A*'s most recent $> 1000\,M_\odot$ companion to within 10 pc of the GC must have occurred no more recently than 324 Myr ago. Extending the known relationship between SMBH masses and the central velocity dispersion of galaxies (Ferrarese & Merritt 2000; Tremaine et al. 2002) to lower masses implies that within this time, the NSC has not accreted any cluster with a central velocity dispersion more than 15 km s^{-1}. Interpolating the relationship between central velocity dispersion and total mass among Milky Way globular clusters in the catalogue of Baumgardt & Hilker (2018), this corresponds to a maximum total cluster mass of $\sim 0.5 - 1 \times 10^6\,M_\odot$. This simple estimate, though not rigorous, shows how HVS observations can be a useful tool for constraining the growth of the Galactic NSC, complementing existing constraints from the identification and modelling of (chemo)kinematic substructures within the NSC (see Feldmeier et al. 2014; Arca Sedda et al. 2020; Do et al. 2020).

3.3 Prospects for DR4 and beyond

Having established constraints on a possible existing or former Sgr A* companion from *Gaia* DR3 HVS observations (or lack thereof), we can explore how these constraints can be updated in the future with the improved astrometric precision and deeper faint-end magnitude limit of *Gaia* DR4, expected $\sim$2026. In the left-hand panel of Fig. 7, we show how constraints the Sgr A* companion mass and either its separation from Sgr A* will change depending on the number of high-confidence HVS uncovered in *Gaia* DR4. The coloured bands show the parameter space allowed if 1, $10 \pm \sqrt{10}$, 100 ± 10, or $1000 \pm \sqrt{1000}$ HVSs are found in DR4. Given the lack of HVSs in *Gaia* DR3, our simulations suggest we should expect no more than 20 HVSs in DR4 if Sgr A* has an existing companion with a mass of $10^3 - 10^4\,M_\odot$, or $\sim$40 HVSs if the companion mass is 10^5. If zero high-confidence HVSs are discovered in *Gaia* DR4, regions of parameter space below the lower edge of the '1' band will be excluded. At fixed separation the maximum allowed companion mass would improve by at least a factor of two. In particular, at smaller separations the upper limit on the mass of a Sgr A* companion would decrease significantly, from $\sim 600\,M_\odot$ to $\sim 150\,M_\odot$.

Similarly, the right-hand panel of Fig. 7 shows how constraints on a former companion to Sgr A* will improve. Former companions more massive than $\sim 500\,M_\odot$, a non-detection of HVSs in *Gaia* DR4 would push the minimum possible time since the MBHB merger will be pushed back by 8 Myr or so. This non-detection would also offer new constraints of Sgr A*'s recent accretion history—it will imply that within the last several Myr Sgr A* can only have accreted a companion no heaver than $\sim$200 $M_\odot$.

Otherwise, since N_{HVS} depends so intimately on M_c and $a_{current}$ or t_{since}, strict (albeit degenerate) constraints can be placed on these parameters if a non-zero number of HVSs are uncovered in the radial velocity catalogue of *Gaia* DR4. In this case, it is, however, important to recognize that the MBHB slingshot mechanism is not the only mechanism that can eject HVSs. Using *all* detected HVSs to constrain a companion to Sgr A* could lead to biased constraints. We discuss this issue in greater detail in the following section.

Beyond *Gaia* DR4, constraints on a possible companion to Sgr A* will improve with HVSs detected (or not) in *Gaia* Data Release 5 (expected $\sim$early 2030s). Throughout the 2030s, improved constraints will also become available via other methods. In particular, observations of the next pericentre passage of the star S2 in 2034 will refine constraints on dark or faint mass within the orbit of S2 (see GRAVITY Collaboration et al. 2022; Heißel et al. 2022). With the launch of LISA in 2037 (Amaro-Seoane et al. 2017), gravitational wave observations of Sgr A* will further constrain the existence of a black hole companion, particularly in the range $10^3 M_\odot \lesssim M_c \lesssim 10^5\,M_\odot$ and $0.1\,\mathrm{mpc} \lesssim a_{current} \lesssim 2\,\mathrm{mpc}$ (Strokov, Fragione & Berti 2023).

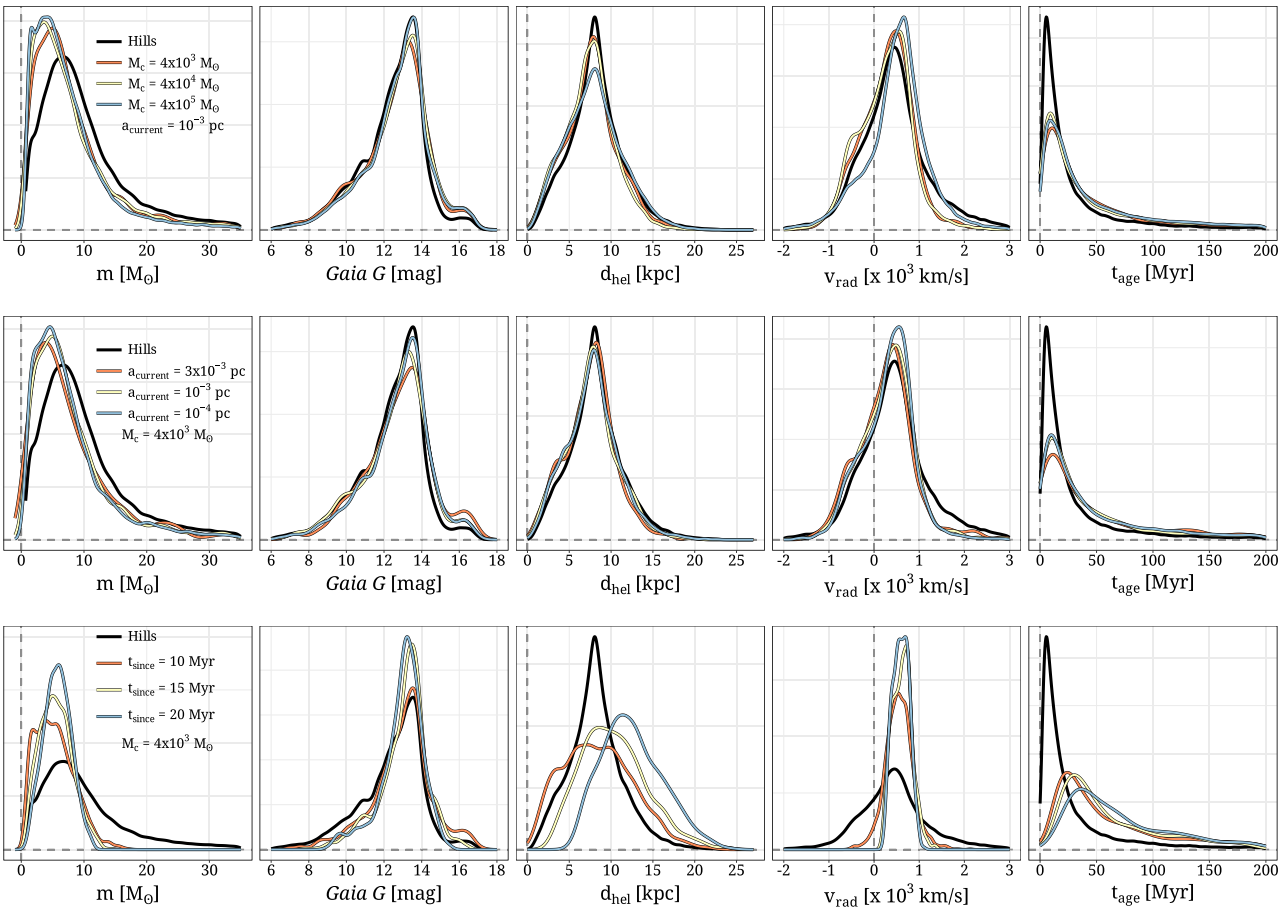

Figure 8. Among HVSs detectable in *Gaia* DR4, distributions of HVS stellar mass m, *Gaia G*-band magnitude, heliocentric distance $d_{\rm hel}$, line-of-sight velocity $v_{\rm rad}$, and HVS stellar age $t_{\rm age}$. Black curves show distributions for HVSs ejected via the Hills mechanism and coloured curves show distributions for HVSs ejected via the MBHB slingshot mechanism when the companion mass (top row), MBHB separation (middle row), and time since the MBHB merger (bottom row) are varied.

4 DISCUSSION

4.1 Contribution from the Hills mechanism

The results of the previous section assume that *all* detectable HVSs are ejected via the MBHB slingshot mechanism. This is not necessarily (nor is it expected to be) true, as multiple possible HVS ejection mechanisms exist and given a sizeable HVS population it may be difficult to disentangle, which was ejected via which mechanism. These other possible mechanisms include the dynamical encounters between single stars and a 'swarm' of stellar-mass black holes in the GC (O'Leary & Loeb 2007) or dynamical interactions between a single SMBH or MBHB and a globular cluster which has sunk toward the GC (Capuzzo-Dolcetta & Fragione 2015; Fragione & Capuzzo-Dolcetta 2016). Most notable among these alternative mechanisms, however, is the Hills mechanism (Hills 1988; Gould & Quillen 2003; Yu & Tremaine 2003), which involves the tidal separation of a stellar binary following a close encounter with a single SMBH. Indeed, it is difficult to contrive a scenario wherein ejections via the MBHB slingshot ejection occur but ejections via the Hills mechanism do not. While there are intrinsic differences in the spatial and velocity distributions of HVSs ejected via the two mechanisms (see Brown 2015; Rasskazov et al. 2019, and references therein), in practice this is difficult to discern directly, given that current observations can detect only a biased subsample of these populations, i.e. those which are bright and relatively nearby.

When considering *null* HVS, disentangling HVS ejection mechanisms is not a problem, as a complete dearth of HVSs can constrain all ejection mechanisms simultaneously. For *non-null* detections, however, as may be the case for *Gaia* DR4, this should be considered. Confident constraints on an HVS ejection mechanisms cannot be imposed using a particular HVS candidate without a notion of which mechanism(s) may be responsible ejecting it. The HVS candidate S^5-HVS1 is an example of this conundrum, and the next subsection below will be devoted to it. While it is beyond the scope of this work to develop a fully self-consistent ejection model including both the Hills mechanism and the MBHB mechanism simultaneously, in this subsection we consider whether HVS populations ejected via these different mechanisms can be meaningfully disentangled.

To compare the two populations, we use a population of Hills mechanism-ejected HVSs generated by Marchetti et al. (2022). We refer the reader to that work for more details concerning the generation of this catalogue, but it assumes an IMF index among HVS progenitors of $\kappa = -1.7$ and generates HVS progenitor binaries assuming power-law distributions of the binary mass ratio and log-orbital period. In Fig. 8, we compare the properties of the *Gaia* DR4-detectable HVS population ejected via the Hills mechanism (black) to the population ejected via the MBHB slingshot mechanism

(orange/yellow/blue). Shown are the distributions of the detectable stars' stellar masses, *Gaia* *G*-band magnitudes, heliocentric distances, heliocentric radial velocities, and stellar ages, stacked over 40 iterations. When we vary M_c or $a_{current}$ (top and middle rows), differences between the populations are subtle. Hills-ejected HVSs are on average slightly more massive and younger than MBHB slingshot-ejected ones, and if the Sgr A* companion is particularly massive and/or its separation from Sgr A* is small, slingshot-ejected HVSs will on average exhibit a narrower range of radial velocities and will span a wider range of distances. If Sgr A* and its companion have already merged, differentiating between the mechanisms becomes easier. The bottom row of Fig. 8 shows that as the time t_{since} since coalescence increases, the range of stellar masses among detectable MBHB slingshot-ejected HVSs narrows (the most massive HVSs will have died, low-mass HVSs will be too far away to detect), the typical distance increases (this final 'gasp' of HVSs will be further away), the range of radial velocities narrows (they are less impacted by the Galactic potential and farther away, so their velocity is more in the radial direction) and their typical ages increase (they cannot be younger than t_{since}). However, given that we expect 5^{+11}_{-4} Hills mechanism-ejected HVSs in the radial velocity catalogue of *Gaia* DR4 (Evans et al. 2022b) and *at most* a few tens of MBHB slingshot-ejected HVSs (Fig. 7), uncontroversially assigning each HVS to a corresponding ejection mechanism will be difficult in any case.

It should be noted as well that the spatial distribution of HVSs could also help discriminate between ejection mechanisms. We assume MBHB-ejected stars are ejected isotropically from the GC, when in reality the fastest stars should be ejected parallel to the plane of the binary and ejections become more isotropic as the MBHB spirals in (Sesana et al. 2006). In Section 4.3, we comment further on how this impacts our results. Since ejections via the Hills mechanism are isotropic, an obvious anisotropy in the spatial distribution of Galactic HVSs would be a clear indication that another mechanism is at work. A significant overdensity of HVS candidates in the direction of Leo was first reported by Brown et al. (2009b), and this apparent overdensity has persisted even as new HVS candidates have been discovered and others discarded (see Boubert et al. 2018). Most of the HVS candidates in this overdensity have ambiguous origins, however, and a satisfying explanation for the overdensity does not yet exist—it is not clear whether it is real or simply the result of observational biases.

4.2 The case of S^5-HVS1

Thus far in this work, the only HVS observational data we have considered is the lack of high-quality HVS candidates in *Gaia* DR3. Both null *and* non-null HVS detections exist in other searches and surveys, however, which can in principle strengthen constraints. For example, the MMT HVS Survey (Brown et al. 2009a, 2012, 2014) identified several dozen HVS candidates. We choose not to include these in our analysis since proper motion measurements for these candidates are not sufficiently precise to conclusively associate any with an ejection from the GC.[12] Liao et al. (2023) identified two stars in the *Gaia* DR3 radial velocity catalogue, *Gaia* DR3 6016819861087891456 and *Gaia* DR3 4094201527955913856, which are currently travelling at high velocities ($v_{total} \approx 600\,km\,s^{-1}$) and appear to have passed within 1 kpc of the GC within the last several Myr. The location of the GC, however, still lies outside the range of possible past trajectories of these stars given current astrometric and radial velocity uncertainties, so the origins of these interesting stars remain ambiguous. For this reason, we choose not to include these stars in our analysis.

Worth mentioning as well is the HVS candidate S5-HVS1, a $\sim 2.35\,M_\odot$ star first identified by Koposov et al. (2020) in the S^5 survey (Li et al. 2019). S^5-HVS1 is notable in that it is the first HVS candidate for whom an origin in the GC is uncontroversial—its trajectory points directly away from the GC and implies an ejection 4.8 Myr ago with a velocity of $v_{ej} \simeq 1800\,km\,s^{-1}$. As an unambiguous HVS detection, we showed in Evans et al. (2022b) that penalizing models which predict zero or $\gg$1 HVSs similar to S^5-HVS1 in the S^5 survey significantly improved constraints on the IMF slope in the GC and the ejection rate of HVSs via the Hills mechanism. In this subsection, we comment on how and whether the inclusion of this star can improve constraints on a current of former companion to Sgr A*.

To identify mock HVSs, which would have appeared as promising HVSs in S^5 by the analysis of Koposov et al. (2020), we first compute each star's apparent magnitude in the Dark Energy Camera (DECam) g and r bands (Abbott et al. 2018) using the `MIST` models as done in Section 2.3. We then roughly reproduce the S^5 selection function, selecting HVSs within the S^5 sky footprint (see Li et al. 2019, table 2) which have *Gaia* parallaxes satisfying $\varpi < 3\sigma_\varpi + 0.2$, and DECam photometry satisfying $15 < g < 19.5$ and $-0.4 < (g-r) < +0.1$. We then take only those mock HVSs with heliocentric radial velocities larger than $800\,km\,s^{-1}$, since these were the ones selected for further inspection by Koposov et al. (2020).

The results of these selections are shown in Fig. 9. Assuming the MBHB slingshot mechanism is the only mechanism ejecting HVSs, the left-hand panel colourbar shows the number of S^5-HVS1 analogues predicted to appear in S^5 depending on the Sgr A* companion mass and the current separation of the MBHB. Configurations between the white lines are consistent within 1σ with finding exactly one star similar to S^5-HVS1 in S^5, and herein lies the issue: a majority of these configurations exist within the parameter space already excluded by the lack of HVSs in the radial velocity catalogue of *Gaia* DR3. Assuming the MBHB slingshot mechanism is responsible for S^5-HVS1, the lack of HVSs in *Gaia* DR3 and the existence of S^5-HVS1 would constrain an existing MBHB in the GC to a degenerate but quite narrow strip of configurations in the range $300\,M_\odot \lesssim M_c \lesssim 7000\,M_\odot$ and $a_{current} \lesssim 5$ mpc.

In the right-hand panel, we show similar results in $M_c - t_{since}$ space. Sgr A* having merged within the last few tens of Myr with a $\sim 300 - 4000\,M_\odot$ companion is consistent with both the existence of S^5-HVS1 and the lack of HVSs in DR3. Note, however, that S^5-HVS1 has a well-constrained flight time of 4.8 Myr. If it were ejected via the MBHB slingshot mechanism shortly before a merger, this merger must have occurred at most 4.8 Myr ago. Within this time-frame, only a $300\,M_\odot \lesssim M_c \lesssim 500\,M_\odot$ companion can reconcile the existence of an HVS in S^5 with the non-detection of HVSs in *Gaia* DR3.

In conclusion, our simulations only support a MBHB slingshot origin for S^5-HVS1 in specific circumstances. Additionally, our criteria to select S^5-HVS1 analogues above makes no consideration for its extreme Galactocentric velocity of $1750\,km\,s^{-1}$. A velocity this large is quite hard to achieve in the MBHB slingshot mechanism for a companion mass of $\lesssim 500\,M_\odot$—only ~20 per cent of our S^5-HVS1 analogues in this mass range are as fast as S^5-HVS1. Typical ejection velocities via the Hills mechanism, on the other hand, are comparatively larger and can more easily accommodate this star. A more rigourous investigation of whether S^5-HVS1 could be produced

[12]Note, however, that unless one invokes an interaction with a massive black hole, it becomes quite difficult to explain the extreme velocities of young HVS candidates with well-constrained total velocities such as HVS1 (Brown et al. 2005).

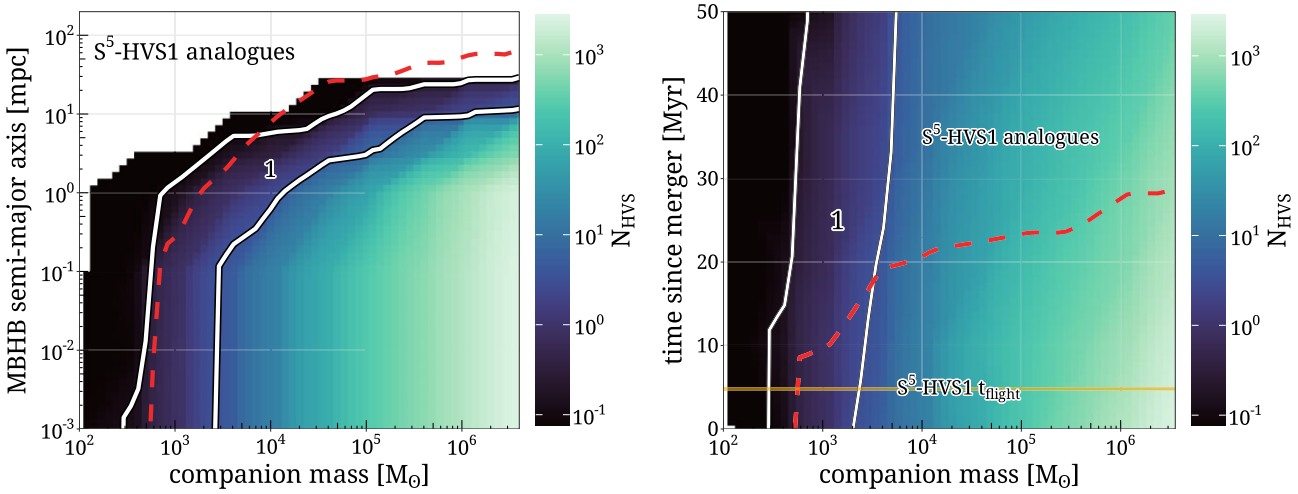

Figure 9. The colourbar shows the population of HVSs predicted to appear in the S^5 survey (see Section 4.2 for details) in both M_c-vs-$a_{current}$ space (left-hand panel) and M_c-vs-t_{since} space (right-hand panel). Configurations below the red dashed lines are excluded by the results of this work. The white, hashed areas show regions of parameter space consistent with finding exactly one HVS in S^5. The gold horizontal line in the right plot shows the inferred S^5-HVS1 flight time of 4.8 Myr (Koposov et al. 2020).

by this mechanism is warranted and does not yet exist. Generozov & Madigan (2020) used S^5-HVS1's flight time as an observational constraint and found that a 1000 $M_\odot$ companion separated from Sgr A* by 0.01 pc could efficiently reproduce the observed eccentricity distribution of the S-star cluster in the GC. This, however, does not necessarily imply S^5-HVS1 was ejected via the MBHB slingshot mechanism.

4.3 The impact of model simplifications

Our model for the ejection of HVSs from the MBHB slingshot mechanism includes a number of implicit and explicit simplifying assumptions. Works in recent years have shown that some of these assumptions (i) impact the evolution of MBHBs and (ii) may not hold strictly true in the centre of our own Galaxy. In this subsection, we comment on the degree to which our results could be impacted by these simplifications.

We assume that our MBHB is non-accreting and in a gas-free environment. Dynamical friction driven by a dense gaseous disc and accretion onto the MBHB impact the separation, eccentricity and inclination evolution of the MBHB (see Escala et al. 2005; Dotti, Colpi & Haardt 2006; Dotti et al. 2007; Muñoz, Miranda & Lai 2019) and would influence the stellar evolution of HVS progenitors (see Cantiello, Jermyn & Lin 2021). Accretion onto an MBHB in our own Galaxy would not be strong enough to impact its evolution—X-ray observations of the GC indicate an accretion rate of $10^{-6} - 10^{-5}\,M_\odot\,yr^{-1}$ (Baganoff et al. 2003; Quataert 2004) at the Bondi radius (0.04 pc) and polarization measurements limit the accretion rate to $\sim 10^{-8}\,M_\odot\,yr^{-1}$ near the Schwarzschild radius (Quataert & Gruzinov 2000; Bower et al. 2003; Marrone et al. 2007). We can check the impact of this accretion with a back of the envelope calculation. Assuming that the inspiral of a MBHB is driven entirely by gas accretion, differentiating the angular momentum of the MBHB with respect to time yields

$$\frac{\dot{a}}{a} = 2\left(\frac{\dot{\ell}}{\ell} - \frac{3}{2}\right)\frac{\dot{M}}{M}\,, \tag{16}$$

where $\dot{a}$ is the hardening rate, $\dot{M}$ is the rate of accretion onto the MBHB, M is the total MBHB mass and $\ell = L/M$ is the specific angular momentum of the binary. $2(\dot{\ell}/\ell - 3/2)$ is a constant of order unity depending on gas accretion physics (see D'Orazio & Duffell 2021). Plugging in characteristic numbers for the accretion rate and MBHB mass, the accretion-driven hardening rate is always at least ten orders of magnitude smaller than the total slingshot + gravitational wave hardening rate. While evidence exists for an episode of nuclear activity in the GC in the last few Myr (see Bland-Hawthorn et al. 2019, and references therein), this flare was short-lived. On the scale of detectable HVS flight times, it is valid to assume a putative MBHB in the GC would be non-accreting and in a gas-poor environment. See Naoz et al. (2020) for further discussion on the impact of accretion on a presumed black hole companion to Sgr A*.

We have assumed for simplicity that the presumed MBHB in the GC is on an initially circular orbit and never deviate from a circular orbit until coalescence. This assumption is valid since the impact of eccentricity on the ejected HVS population is ultimately quite minor (Quinlan 1996; Sesana et al. 2006). Rasskazov et al. (2019) show that non-zero eccentricity increases the binary hardening rate H by up to ~10 per cent at separations below the hardening separation, but at larger separations the hardening rate is largely unchanged. The mass ejection rate J of the MBHB slingshot mechanism very shortly before coalescence can increase by up to ~20 per cent if the binary is very eccentric, but for separations $0.1 < a/a_h < 1$ the mass ejection rate of a highly eccentric MBHB is actually lower than that of a circular binary. In any case, the impact of eccentricity is only relevant in the first place for MBHB mass ratios larger than 10^{-3} – smaller mass ratio MBHBs tend to circularize with time (Rasskazov et al. 2019; Bonetti et al. 2020).

Our model of the GC assumes the MBHB is embedded within a spherical, non-rotating NSC. In actuality, the NSC is slightly flattened along the Galactic vertical axis (Schödel et al. 2014) and rotates more or less parallel with the Galactic disc (Trippe et al. 2008; Schödel et al. 2009; Chatzopoulos et al. 2015; Fritz et al. 2016). A nuclear cluster, which co-(counter-)rotates with the MBHB enhances (suppresses) eccentricity growth of the MBHB (Sesana, Gualandris & Dotti 2011; Rasskazov & Merritt 2017; Rasskazov et al. 2019; Bonetti et al. 2020) while the impact of counter- and co-rotation of the NSC on the MBHB hardening rate is less clear (see contradictory results in Holley-Bockelmann & Khan 2015; Mirza

et al. 2017; Rasskazov & Merritt 2017; Rasskazov et al. 2019; Varisco et al. 2021). A maximally co-rotating nucleus decreases the mass ejection rate J by ∼10 per cent at small separations ($a \lesssim 0.3a_{\rm h}$) relative to a non-rotating nucleus (Rasskazov et al. 2019), in which case our assumption of a non-rotating NSC may be overestimating $N_{\rm HVS}$. If the NSC is maximally counter-rotating, however, the mass ejection rate at small separations is increased by a factor of up to ∼40 per cent (Rasskazov et al. 2019). This is less of a concern, given that MBHBs are expected to align their rotation with the angular momentum of the NSC (see below).

The density ρ and velocity dispersion σ of the NSC impact the MBHB hardening rate (equations 1–3); we assume single values for these, when in fact they both vary with radial distance from the GC (Schödel et al. 2009, 2014; Feldmeier et al. 2014). We have confirmed that variations of σ and ρ within observational uncertainties do not meaningfully affect the results of this work. Along with this, we neglect to consider mass segregation as well within the NSC. A mass segregated stellar environment accelerates hardening timescales among highly unequal-mass MBHBs but has the opposite impact on ∼equal mass MBHBs (Mukherjee et al. 2023). We assume as well that the MBHB centre of mass is always centred on the exact geometric centre of the Galaxy. In reality, the MBHB will 'drift' randomly in a non-rotating stellar nucleus (Merritt 2001; Chatterjee, Hernquist & Loeb 2003) or on a closed orbit if the nucleus is rotating (Holley-Bockelmann & Khan 2015; Mirza et al. 2017; Khan, Mirza & Holley-Bockelmann 2020; Varisco et al. 2021). The center of mass displacement from the Galactic barycentre is typically on the order of the MBHB radius of influence or smaller, i.e. not large enough to meaningfully affect the detectable HVS population. There are very few cases where shifting the positions of a *Gaia*-detectable mock HVS by ∼a few pc in any direction renders it undetectable.

When generating mock HVS populations, we take no consideration of the orientation and phase of the MBHB. If stars are ejected isotropically in the MBHB slingshot mechanism, the orientation of the MBHB is irrelevant. While our model assumes isotropic ejection, theoretical treatments predict that the fastest-ejected stars are ejected preferentially in the plane of the binary, with a complex polar angle distribution depending on its separation, eccentricity, and mass ratio (Sesana et al. 2006; Darbha et al. 2019; Rasskazov et al. 2019). Ejections are likely non-axisymmetric as well, though the azimuthal distribution of fast ejections remains unclear (see discussion in Rasskazov et al. 2019). Without independent constraints on the inclination/phase of the MBHB, we would be compelled to sample them at random, and therefore any angular dependence would get washed out in our results after averaging over many iterations. There is reason to believe, however, that a putative MBHB in the GC would be aligned with the Galactic disc. For a spherical, non-rotating NSC, the orientation of the MBHB orbit drifts on the order of $\sqrt{m_*/M_{\rm MBHB}} \sim 10^{-4}$ rad relative to its initial orientation, where m_* is the typical mass of a star in the NSC and $M_{\rm MBHB}$ is the total mass of the MBHB (Merritt 2001). In a rotating NSC, however, the angular momentum of the MBHB aligns with the angular momentum of the nucleus (Gualandris, Dotti & Sesana 2012; Cui & Yu 2014; Wang et al. 2014; Rasskazov & Merritt 2017). Having established above that the Milky Way NSC rotates parallel to the Galactic disc, it is not unreasonable to assume a putative MBHB would rotate parallel with the disc as well. Another point in favour of this is the existence of the nuclear stellar disc embedded within the NSC itself (Bartko et al. 2009; Lu et al. 2009; Yelda et al. 2014). This stellar disc rotates in the direction of the overall Galactic disc as well (Schönrich, Aumer & Sale 2015; Schultheis et al. 2021; Sormani et al. 2022) and resonant relaxation processes would align any IMBH–SMBH binary with such a disc (Szölgyén, Máthé & Kocsis 2021; Magnan et al. 2022). If the MBHB orbit were indeed aligned with the Galactic mid-plane, our assumption of isotropic ejections would slightly underestimate $N_{\rm HVS}$, since in actuality a greater proportion of HVSs are ejected on angles pointed more flattened toward the Earth. We note that our simulations in this work only consider the interactions between single stars isotropically approaching an MBHB in the GC. The presence of other perturbers in the GC region including molecular clouds, infalling globular clusters, or additional IMBH companions are not considered and could have a large impact on the evolution of the MBHB and the ejection of HVSs. This is not such a concern for massive companions to Sgr A*, but is worth consideration for $M_{\rm c} \lesssim 1000$ companions. If Sgr A* were to have such a low-mass companion, it is entirely possible for it to be in a higher-order system with one or more additional black hole companions. Further modelling work would be required to accurately model the population of HVSs ejected by such a system.

Finally, our model assumes the phase space of low-angular momentum orbits, which bring GC stars on a close ($\lesssim a$) approach to the MBHB is efficiently repopulated over time. Only stars within this 'loss cone' experience strong dynamical interaction with the MBHB. This loss cone is refilled over time, primarily via two-body relaxation in the NSC Sgr A* (see Lightman & Shapiro 1977; Merritt 2013) or resonant relaxation processes in the young clockwise disc (Rauch & Tremaine 1996; Madigan, Levin & Hopman 2009; Madigan, Hopman & Levin 2011; Madigan et al. 2014). If these scattering mechanisms are not efficient, the loss cone can empty and the MBHB hardening (and therefore the ejections of HVSs) can slow down or cease entirely (Milosavljević & Merritt 2003). This problem was investigated in the context of HVS ejections by Sesana, Haardt & Madau (2007b), who found that without loss cone refilling the MBHB stalls after ejecting only half the MBHB reduced mass in stars, $\sim 10^2 - 10^6\,{\rm M}_\odot$ in our case depending on the assumed mass ratio. This is smaller than the total mass ejected in the full loss cone regime by a factor of a few (∼10) if the mass ratio is small (large) and the ejected stars would have smaller typical velocities. Concerns about loss cone depletion among MBHBs has largely been alleviated in recent years, as simulations have shown that relaxation-driven refilling of the loss cone is sufficient to avoid loss cone depletion in triaxial potentials (Berczik et al. 2006; Vasiliev, Antonini & Merritt 2015; Gualandris et al. 2017), or even biaxial potentials (Khan et al. 2013). Regardless, our models in this work assume a full loss cone, and this can lead to an overestimation of $N_{\rm HVS}$ in cases of partial depletion. This assumption is likely the largest source of systematic uncertainty in our modelling. Given the strong dependence of $N_{\rm HVS}$ large range of HVS population sizes As noted by Vasiliev et al. (2015), it is relatively straightforward to adjust H and J (equation (9)) to account for loss cone depletion (see also Rasskazov et al. 2019).

5 CONCLUSIONS

MBHBs are a natural consequence of galaxy evolution. Dynamical interactions between stars and an MBHB in the centre of the Milky Way could eject hypervelocity stars (HVSs) detectable by the *Gaia* space satellite. In this work, we use existing HVS observations for the first time as a probe of a possible supermassive or intermediate mass companion black hole to Sgr A*, the supermassive black hole located in the GC. Building upon previous work, we realistically simulate the ejection of HVSs from an MBHB assuming a variety of MBHB mass ratios and separations. We focus in particular on HVSs, which would have appeared in the radial velocity catalogue

of the third data release from *Gaia*. Considering that zero HVSs with precise astrometry were unearthed in the radial velocity catalogue of *Gaia* DR3 (Marchetti et al. 2022), MBHB configurations which predict too many HVSs in this data release can be excluded. Our conclusions are as follows:

(i) The number of HVSs detectable by *Gaia* depends strongly on the MBHB separation and companion mass. It is comparatively less sensitive to the shape of the assumed IMF (Fig. 3).
(ii) For a fiducial Sgr A* companion mass of 4000 $M_\odot$ and MBHB separation of 0.001 pc, 9 ± 3 HVSs should have been detected in the *Gaia* DR3 radial velocity catalogue with precise astrometry (Fig. 4).
(iii) The *lack* of such HVSs in DR3 excludes a companion within 1 mpc of Sgr A* unless it has a mass of $\lesssim 2000\,M_\odot$, complementing and extending prior constraints on a Sgr A* companion (Fig. 5).
(iv) The lack of confident HVS detections in *Gaia* DR3 also allows us to constrain a *former* companion to Sgr A* for the first time. If Sgr A* merged with a companion in the recent past, either of the following must be true: (i) the former companion had a mass of $\lesssim 500\,M_\odot$, or (ii) the merger must have happened more than ∼10–30 Myr ago (Fig. 6).
(v) If Sgr A* has an existing companion or had a former companion, the forthcoming fourth *Gaia* data release will contain at most a few tens of HVSs ejected via the MBHB slingshot mechanism in its radial velocity catalogue with precise astrometry (Fig. 7).

The constraints we place in this work on a possible companion to Sgr A*, especially when combined with constraints obtained over the last few years (GRAVITY Collaboration et al. 2020; Naoz et al. 2020; Reid & Brunthaler 2020), appear to be closing the door on the existence of such a companion. While a massive companion up to $\sim 10^5 M_\odot$ is still allowed at separations larger than ~ 0.1 pc, a hardened MBHB in the GC appears unlikely unless the MBHB mass ratio is extreme. With the future *Gaia* data releases and their synergy with both forthcoming and currently operational spectroscopic facilities and surveys (e.g. WEAVE; Dalton et al. 2012, 4MOST; de Jong et al. 2019, SDSS-V MWM; Kollmeier et al. 2017), more and more HVSs will be detected. If Sgr A* does not have a companion of significant mass and did not have one in the recent past, the MBHB slingshot mechanism can be definitely ruled out as an avenue for HVS ejections and future research can focus on more realistic mechanisms.

ACKNOWLEDGEMENTS

The authors thank the anonymous referee for their helpful feedback. We thank J.R. Westernacher-Schneider for helpful discussion. FAE acknowledges support from the University of Toronto Arts & Science Post-doctoral Fellowship program and the Dunlap Institute. TM acknowledges an ESO fellowship. EMR acknowledges that this project has received funding from the European Research Council (ERC) under the European Union's Horizon 2020 research and innovation programme (grant agreement number 101002511—VEGA P). JB acknowledges financial support from NSERC (funding reference number RGPIN-2020-04712).

DATA AVAILABILITY

The simulation outputs underpinning this work can be shared upon reasonable request to the corresponding author. The simulations analysed in this work were produced using the publicly available `PYTHON` package `speedystar` (https://github.com/fraserevans/speedystar).

REFERENCES

Abbott T. M. C. et al., 2018, ApJS, 239, 18
Akiyama K. et al., 2022, ApJ, 930, L15
Amaro-Seoane P. et al., 2017, preprint (arXiv:1702.00786)
Antonini F., Gieles M., Gualandris A., 2019, MNRAS, 486, 5008
Arca Sedda M., Gualandris A., Do T., Feldmeier-Krause A., Neumayer N., Erkal D., 2020, ApJ, 901, L29
Arca-Sedda M., Gualandris A., 2018, MNRAS, 477, 4423
Askar A., Davies M. B., Church R. P., 2021, MNRAS, 502, 2682
Atallah D., Trani A. A., Kremer K., Weatherford N. C., Fragione G., Spera M., Rasio F. A., 2023, MNRAS, 523, 4227
Baganoff F. K. et al., 2003, ApJ, 591, 891
Bailer-Jones C. A. L., 2015, PASP, 127, 994
Ballone A., Costa G., Mapelli M., MacLeod M., Torniamenti S., Pacheco-Arias J. M., 2023, MNRAS, 519, 5191
Bartko H. et al., 2009, ApJ, 697, 1741
Baumgardt H., Gualandris A., Portegies Zwart S., 2006, MNRAS, 372, 174
Baumgardt H., Hilker M., 2018, MNRAS, 478, 1520
Begelman M. C., Blandford R. D., Rees M. J., 1980, Nature, 287, 307
Bennett M., Bovy J., 2019, MNRAS, 482, 1417
Berczik P., Merritt D., Spurzem R., Bischof H.-P., 2006, ApJ, 642, L21
Bessell M. S., 1990, PASP, 102, 1181
Bland-Hawthorn J. et al., 2019, ApJ, 886, 45
Bonetti M. et al., 2020, MNRAS, 493, L114
Boubert D., Guillochon J., Hawkins K., Ginsburg I., Evans N. W., Strader J., 2018, MNRAS, 479, 2789
Bovy J., 2015, ApJS, 216, 29
Bovy J., Rix H.-W., Green G. M., Schlafly E. F., Finkbeiner D. P., 2016, ApJ, 818, 130
Bower G. C., Wright M. C. H., Falcke H., Backer D. C., 2003, ApJ, 588, 331
Bromley B. C., Kenyon S. J., Brown W. R., Geller M. J., 2018, ApJ, 868, 25
Brown A. G. A., 2019, 53rd ESLAB Symposium: The Gaia Universe. Noordwijk, the Netherlands, p. 18
Brown W. R., 2015, ARA&A, 53, 15
Brown W. R., Geller M. J., Kenyon S. J., 2009a, ApJ, 690, 1639
Brown W. R., Geller M. J., Kenyon S. J., Bromley B. C., 2009b, ApJ, 690, L69
Brown W. R., Geller M. J., Kenyon S. J., 2012, ApJ, 751, 55
Brown W. R., Geller M. J., Kenyon S. J., 2014, ApJ, 787, 89
Brown W. R., Geller M. J., Kenyon S. J., Kurtz M. J., 2005, ApJ, 622, L33
Brown W. R., Geller M. J., Kenyon S. J., Kurtz M. J., 2006, ApJ, 640, L35
Cantat-Gaudin T. et al., 2022, A&A, 669, 20
Cantiello M., Jermyn A. S., Lin D. N. C., 2021, ApJ, 910, 94
Capuzzo-Dolcetta R., Fragione G., 2015, MNRAS, 454, 2677
Castro-Ginard A. et al., 2023, preprint (arXiv:2303.17738)
Chandrasekhar S., 1943, ApJ, 97, 255
Chatterjee P., Hernquist L., Loeb A., 2003, ApJ, 592, 32
Chatzopoulos S., Fritz T. K., Gerhard O., Gillessen S., Wegg C., Genzel R., Pfuhl O., 2015, MNRAS, 447, 948
Choi J., Dotter A., Conroy C., Cantiello M., Paxton B., Johnson B. D., 2016, ApJ, 823, 102
Cropper M. et al., 2018, A&A, 616, A5
Cui X., Yu Q., 2014, MNRAS, 437, 777
D'Orazio D. J., Duffell P. C., 2021, ApJ, 914, L21
Dalton G. et al., 2012, in McLean I. S., Ramsay S. K., Takami H., eds, Proc. SPIE Conf. Ser.Vol. 8446, Ground-based and Airborne Instrumentation for Astronomy IV. SPIE, Bellingham, p. 84460P
Darbha S., Coughlin E. R., Kasen D., Quataert E., 2019, MNRAS, 482, 2132
de Jong R. S. et al., 2019, The Messenger, 175, 3
Di Matteo T., Springel V., Hernquist L., 2005, Nature, 433, 604
Do T., David Martinez G., Kerzendorf W., Feldmeier-Krause A., Arca Sedda M., Neumayer N., Gualandris A., 2020, ApJ, 901, L28
Dormand J., Prince P., 1980, J. Comput. Appl. Math., 6, 19
Dotter A., 2016, ApJS, 222, 8
Dotti M., Colpi M., Haardt F., 2006, MNRAS, 367, 103
Dotti M., Colpi M., Haardt F., Mayer L., 2007, MNRAS, 379, 956
Drimmel R., Cabrera-Lavers A., López-Corredoira M., 2003, A&A, 409, 205

Drimmel R., Poggio E., 2018, Res. Notes Am. Astron. Soc., 2, 210
Du C., Li H., Yan Y., Newberg H. J., Shi J., Ma J., Chen Y., Wu Z., 2019, ApJS, 244, 4
Eisenhauer F. et al., 2005, Apj, 628, 246
El-Badry K. et al., 2023, The Open Journal of Astrophysics, 6, 28
Escala A., Larson R. B., Coppi P. S., Mardones D., 2005, ApJ, 630, 152
Evans F. A., Marchetti T., Rossi E. M., 2022a, MNRAS, 512, 2350
Evans F. A., Marchetti T., Rossi E. M., 2022b, MNRAS, 517, 3469
Everall A., Boubert D., 2022, MNRAS, 509, 6205
Everall A., Boubert D., Koposov S. E., Smith L., Holl B., 2021, MNRAS, 502, 1908
Fabricius C. et al., 2021, A&A, 649, A5
Feldmeier A. et al., 2014, A&A, 570, A2
Ferrarese L., Merritt D., 2000, ApJ, 539, L9
Figer D. F. et al., 2003, ApJ, 599, 1139
Fouvry J.-B., José Bustamante-Rosell M., Zimmerman A., 2023, preprint (arXiv:2305.15998)
Fragione G., 2022, ApJ, 939, 97
Fragione G., Capuzzo-Dolcetta R., 2016, MNRAS, 458, 2596
Fragione G., Kocsis B., Rasio F. A., Silk J., 2022a, ApJ, 927, 231
Fragione G., Loeb A., Kocsis B., Rasio F. A., 2022b, ApJ, 933, 170
Fritz T. K. et al., 2016, ApJ, 821, 44
Gaia Collaboration et al., 2016, A&A, 595, A2
Gaia Collaboration et al., 2021, A&A, 649, A1
Gaia Collaboration et al., 2022, A&A, 674, 22
Generozov A., 2021, MNRAS, 501, 3088
Generozov A., Madigan A.-M., 2020, ApJ, 896, 137
Genzel R., Eisenhauer F., Gillessen S., 2010, Rev. Mod. Phys., 82, 3121
Ghez A. M. et al., 2008, ApJ, 689, 1044
Gillessen S., Eisenhauer F., Trippe S., Alexander T., Genzel R., Martins F., Ott T., 2009, ApJ, 692, 1075
González E., Kremer K., Chatterjee S., Fragione G., Rodriguez C. L., Weatherford N. C., Ye C. S., Rasio F. A., 2021, ApJ, 908, L29
Gould A., Quillen A. C., 2003, ApJ, 592, 935
GRAVITY Collaboration et al., 2018, A&A, 615, L15
GRAVITY Collaboration et al., 2020, A&A, 636, L5
GRAVITY Collaboration et al., 2022, A&A, 657, L12
GRAVITY Collaboration et al., 2023, A&A, 672, A63
Green G. M. et al., 2015, ApJ, 810, 25
Greene J. E., Strader J., Ho L. C., 2020, ARA&A, 58, 257
Gualandris A., Dotti M., Sesana A., 2012, MNRAS, 420, L38
Gualandris A., Gillessen S., Merritt D., 2010, MNRAS, 409, 1146
Gualandris A., Merritt D., 2009, ApJ, 705, 361
Gualandris A., Portegies Zwart S., Sipior M. S., 2005, MNRAS, 363, 223
Gualandris A., Read J. I., Dehnen W., Bortolas E., 2017, MNRAS, 464, 2301
Gürkan M. A., Freitag M., Rasio F. A., 2004, ApJ, 604, 632
Hansen B. M. S., Milosavljević M., 2003, ApJ, 593, L77
Hattori K., Valluri M., Bell E. F., Roederer I. U., 2018, ApJ, 866, 121
Heber U., Edelmann H., Napiwotzki R., Altmann M., Scholz R. D., 2008, A&A, 483, L21
Heißel G., Paumard T., Perrin G., Vincent F., 2022, A&A, 660, A13
Hills J. G., 1988, Nature, 331, 687
Holley-Bockelmann K., Khan F. M., 2015, ApJ, 810, 139
Huang Y. et al., 2017, ApJ, 847, L9
Huang Y., Li Q., Zhang H., Li X., Sun W., Chang J., Dong X., Liu X., 2021, ApJ, 907, L42
Hurley J. R., Pols O. R., Tout C. A., 2000, MNRAS, 315, 543
Igoshev A. P., Perets H., Hallakoun N., 2023, MNRAS, 518, 6223
Irrgang A., Geier S., Heber U., Kupfer T., Fürst F., 2019, A&A, 628, L5
Irrgang A., Przybilla N., Heber U., Nieva M. F., Schuh S., 2010, ApJ, 711, 138
Jordi C. et al., 2010, A&A, 523, A48
Katz D. et al., 2019, A&A, 622, A205
Katz D. et al., 2022, A&A, 674, 31
Kenyon S. J., Bromley B. C., Geller M. J., Brown W. R., 2008, ApJ, 680, 312
Khan F. M., Holley-Bockelmann K., Berczik P., Just A., 2013, ApJ, 773, 100
Khan F. M., Mirza M. A., Holley-Bockelmann K., 2020, MNRAS, 492, 256
Kobayashi S., Hainick Y., Sari R., Rossi E. M., 2012, ApJ, 748, 105
Kollmeier J. A. et al., 2017, preprint (arXiv:1711.03234)
Koposov S. E. et al., 2020, MNRAS, 491, 2465
Kormendy J., Ho L. C., 2013, ARA&A, 51, 511
Levin Y., 2006, ApJ, 653, 1203
Levin Y., Beloborodov A. M., 2003, ApJ, 590, L33
Li H., Du C., Ma J., Shi J., Newberg H. J., Piao Y., 2022, ApJ, 933, L13
Li T. S. et al., 2019, MNRAS, 490, 3508
Li Y.-B. et al., 2018, AJ, 156, 87
Li Y.-B. et al., 2021, ApJS, 252, 3
Liao J., Du C., Li H., Ma J., Shi J., 2023, ApJ, 944, L39
Lightman A. P., Shapiro S. L., 1977, ApJ, 211, 244
Löckmann U., Baumgardt H., Kroupa P., 2008, ApJ, 683, L151
Lu J. R., Do T., Ghez A. M., Morris M. R., Yelda S., Matthews K., 2013, ApJ, 764, 155
Lu J. R., Ghez A. M., Hornstein S. D., Morris M. R., Becklin E. E., Matthews K., 2009, ApJ, 690, 1463
Luna A., Minniti D., Alonso-García J., 2019, ApJ, 887, L39
McKernan B., Ford K. E. S., Kocsis B., Lyra W., Winter L. M., 2014, MNRAS, 441, 900
McKernan B., Ford K. E. S., Lyra W., Perets H. B., 2012, MNRAS, 425, 460
McMillan P. J., 2017, MNRAS, 465, 76
Madigan A.-M., Hopman C., Levin Y., 2011, ApJ, 738, 99
Madigan A.-M., Levin Y., Hopman C., 2009, ApJ, 697, L44
Madigan A.-M., Pfuhl O., Levin Y., Gillessen S., Genzel R., Perets H. B., 2014, ApJ, 784, 23
Magnan N., Fouvry J.-B., Pichon C., Chavanis P.-H., 2022, MNRAS, 514, 3452
Magorrian J. et al., 1998, AJ, 115, 2285
Marchetti T., 2021, MNRAS, 503, 1374
Marchetti T., Contigiani O., Rossi E. M., Albert J. G., Brown A. G. A., Sesana A., 2018, MNRAS, 476, 4697
Marchetti T., Evans F. A., Rossi E. M., 2022, MNRAS, 515, 767
Marchetti T., Rossi E. M., Brown A. G. A., 2019, MNRAS, 490, 157
Marrone D. P., Moran J. M., Zhao J.-H., Rao R., 2007, ApJ, 654, L57
Marshall D. J., Robin A. C., Reylé C., Schultheis M., Picaud S., 2006, A&A, 453, 635
Mastrobuono-Battisti A., Ogiya G., Hahn O., Schultheis M., 2023, MNRAS, 521, 6089
Mastrobuono-Battisti A., Perets H. B., Loeb A., 2014, ApJ, 796, 40
Merritt D., 2001, ApJ, 556, 245
Merritt D., 2013, Dynamics and Evolution of Galactic Nuclei. Princeton Univ. Press, Princeton
Mikkola S., Merritt D., 2008, AJ, 135, 2398
Miller M. C., Hamilton D. P., 2002, MNRAS, 330, 232
Milosavljević M., Merritt D., 2003, ApJ, 596, 860
Mirza M. A., Tahir A., Khan F. M., Holley-Bockelmann H., Baig A. M., Berczik P., Chishtie F., 2017, MNRAS, 470, 940
Mukherjee D., Zhu Q., Ogiya G., Rodriguez C. L., Trac H., 2023, MNRAS, 518, 4801
Muñoz D. J., Miranda R., Lai D., 2019, ApJ, 871, 84
Naoz S., Will C. M., Ramirez-Ruiz E., Hees A., Ghez A. M., Do T., 2020, ApJ, 888, L8
O'Leary R. M., Loeb A., 2007, MNRAS, 383, 86
Palladino L. E., Schlesinger K. J., Holley-Bockelmann K., Allende Prieto C., Beers T. C., Lee Y. S., Schneider D. P., 2014, ApJ, 780, 7
Pelupessy F. I., van Elteren A., de Vries N., McMillan S. L. W., Drost N., Portegies Zwart S. F., 2013, A&A, 557, A84
Peters P. C., 1964, Phys. Rev., 136, 1224
Portegies Zwart S. et al., 2009, New A, 14, 369
Portegies Zwart S. F., McMillan S. L. W., 2002, ApJ, 576, 899
Portegies Zwart S., McMillan S. L. W., van Elteren E., Pelupessy I., de Vries N., 2013, Comput. Phys. Commun., 184, 456
Portegies Zwart S., McMillan S., 2018, Astrophysical Recipes; The art of AMUSE. Institute of Physics Publishing, Bristol
Prudil Z. et al., 2022, A&A, 664, A148
Quataert E., 2004, ApJ, 613, 322
Quataert E., Gruzinov A., 2000, ApJ, 545, 842

Quinlan G. D., 1996, New A, 1, 35
Rasskazov A., Fragione G., Leigh N. W. C., Tagawa H., Sesana A., Price-Whelan A., Rossi E. M., 2019, ApJ, 878, 17
Rasskazov A., Merritt D., 2017, ApJ, 837, 135
Rauch K. P., Tremaine S., 1996, New A, 1, 149
Reid M. J., Brunthaler A., 2004, ApJ, 616, 872
Reid M. J., Brunthaler A., 2020, ApJ, 892, 39
Riello M. et al., 2021, A&A, 649, A3
Rizzuto F. P., Naab T., Spurzem R., Arca-Sedda M., Giersz M., Ostriker J. P., Banerjee S., 2022, MNRAS, 512, 884
Rose S. C., Naoz S., Sari R., Linial I., 2022, ApJ, 929, L22
Rossi E. M., Kobayashi S., Sari R., 2014, ApJ, 795, 125
Sari R., Kobayashi S., Rossi E. M., 2010, ApJ, 708, 605
Sartoretti P. et al., 2022, A&A, 674, 15
Schlafly E. F. et al., 2018, ApJS, 234, 39
Schödel R. et al., 2007, A&A, 469, 125
Schödel R., Feldmeier A., Neumayer N., Meyer L., Yelda S., 2014, Class. Quant. Grav., 31, 244007
Schödel R., Merritt D., Eckart A., 2009, A&A, 502, 91
Schönrich R., Aumer M., Sale S. E., 2015, ApJ, 812, L21
Schultheis M. et al., 2021, A&A, 650, A191
Sesana A., Gualandris A., Dotti M., 2011, MNRAS, 415, L35
Sesana A., Haardt F., Madau P., 2006, ApJ, 651, 392
Sesana A., Haardt F., Madau P., 2007a, MNRAS, 379, L45
Sesana A., Haardt F., Madau P., 2007b, ApJ, 660, 546
Shen K. J. et al., 2018, ApJ, 865, 15
Sormani M. C. et al., 2022, MNRAS, 512, 1857
Speagle J. S., 2020, MNRAS, 493, 3132
Stone N. C., Küpper A. H. W., Ostriker J. P., 2017, MNRAS, 467, 4180
Strokov V., Fragione G., Berti E., 2023, MNRAS, 524, 2033
Szölgyén Á., Máthé G., Kocsis B., 2021, ApJ, 919, 140
Tep K., Fouvry J.-B., Pichon C., Heißel G., Paumard T., Perrin G., Vincent F., 2021, MNRAS, 506, 4289
Tillich A., Przybilla N., Scholz R.-D., Heber U., 2009, A&A, 507, L37
Tremaine S. D., Ostriker J. P., Spitzer L.J., 1975, ApJ, 196, 407
Tremaine S. et al., 2002, ApJ, 574, 740
Trippe S. et al., 2008, A&A, 492, 419
Varisco L., Bortolas E., Dotti M., Sesana A., 2021, MNRAS, 508, 1533
Vasiliev E., Antonini F., Merritt D., 2015, ApJ, 810, 49
Volonteri M., Haardt F., Madau P., 2003, ApJ, 582, 559
Wang L., Berczik P., Spurzem R., Kouwenhoven M. B. N., 2014, ApJ, 780, 164
Yelda S., Ghez A. M., Lu J. R., Do T., Meyer L., Morris M. R., Matthews K., 2014, ApJ, 783, 131
Yu Q., Tremaine S., 2003, ApJ, 599, 1129
Zheng X., Lin D. N. C., Mao S., 2021, ApJ, 914, 33
Zhong J. et al., 2014, ApJ, 789, L2
Zier C., Biermann P. L., 2001, A&A, 377, 23

This paper has been typeset from a TEX/LATEX file prepared by the author.